Collaborative Control of Cell Cycle Progression by the RNA Exonuclease Dis3 and Ras Is Conserved Across Species

Mark J. Snee,* William C. Wilson,† Yi Zhu,* Shin-Yu Chen,‡ Beth A. Wilson,* Cedric Kseib,‡ Julie O'Neal,† Nitin Mahajan,† Michael H. Tomasson,† Swathi Arur,‡,1 and James B. Skeath*,1

*Department of Genetics and †Department of Internal Medicine, Washington University School of Medicine, St. Louis, Missouri 63110, and ‡Department of Genetics, University of Texas MD Anderson Cancer Center, Houston, Texas 77030

ABSTRACT Dis3 encodes a conserved RNase that degrades or processes all RNA species via an N-terminal PilT N terminus (PIN) domain and C-terminal RNB domain that harbor, respectively, endonuclease activity and 3′–5′ exonuclease activity. In *Schizosaccharomyces pombe*, *dis3* mutations cause chromosome missegregation and failure in mitosis, suggesting *dis3* promotes cell division. In humans, apparently hypomorphic *dis3* mutations are found recurrently in multiple myeloma, suggesting *dis3* opposes cell division. Except for the observation that RNAi-mediated depletion of *dis3* function drives larval arrest and reduces tissue growth in *Drosophila*, the role of *dis3* has not been rigorously explored in higher eukaryotic systems. Using the *Drosophila* system and newly generated *dis3* null alleles, we find that absence of *dis3* activity inhibits cell division. We uncover a conserved CDK1 phosphorylation site that when phosphorylated inhibits Dis3's exonuclease, but not endonuclease, activity. Leveraging this information, we show that Dis3's exonuclease function is required for mitotic cell division: in its absence, cells are delayed in mitosis and exhibit aneuploidy and overcondensed chromosomes. In contrast, we find that modest reduction of *dis3* function enhances cell proliferation in the presence of elevated Ras activity, apparently by accelerating cells through G2/M even though each insult by itself delays G2/M. Additionally, we find that *dis3* and *ras* genetically interact in worms and that *dis3* can enhance cell proliferation under growth stimulatory conditions in murine B cells. Thus, reduction, but not absence, of *dis3* activity can enhance cell proliferation in higher organisms.

KEYWORDS Dis3; Ras; cell proliferation; multiple myeloma

DIS3 was initially identified in *Schizosaccharomyces pombe* through a genetic screen for genes required for sister chromatid segregation at mitosis (Ohkura *et al.* 1988). Dis3 belongs to the RNase II family of proteins found in bacteria, archaea, and eukaryotes; this protein family is defined by the presence of a highly conserved RNAse II (RNB) domain (Arraiano *et al.* 2010). The RNB domain degrades single-stranded RNA in a highly processive 3′ to 5′ manner. Dis3 also harbors an N-terminal PilT N terminus (PIN) domain that possesses RNA endonuclease activity (Lebreton *et al.* 2008). Dis3 appears to act as the principle catalytic subunit of the RNA exosome, a large multisubunit protein complex that can degrade and/or process all classes of RNA (Kinoshita *et al.* 1991; Mitchell *et al.* 1997; Dziembowski *et al.* 2007; Lebreton *et al.* 2008; Tomecki *et al.* 2010). Emerging work indicates that noncoding RNAs and RNA processing enzymes, like the RNA exosome, regulate centromere and kinetochore formation and function (Volpe *et al.* 2002; Topp *et al.* 2004; Verdel *et al.* 2004; Buhler *et al.* 2007; Murakami *et al.* 2007; Wong *et al.* 2007; Folco *et al.* 2008; Chan *et al.* 2012; Rosic *et al.* 2014).

In *S. pombe*, the *dis3-54* cold-sensitive mutation reduces RNA exonuclease activity and leads to overcondensed chromosomes that distribute unequally at mitosis, eventually leading to failure or lethality in mitosis (Ohkura *et al.* 1988); elimination of *dis3* activity is incompatible with cell growth in *S. pombe* (Kinoshita *et al.* 1991). Genetic and biochemical studies of *dis3* in vertebrate cells support these findings:

doi: 10.1534/genetics.116.187930
Manuscript received February 3, 2016; accepted for publication March 26, 2016; published Early Online March 30, 2016.
Supplemental material is available online at www.genetics.org/lookup/suppl/doi:10.1534/genetics.116.187930/-/DC1.
[1]Corresponding authors: Department of Genetics, University of Texas MD Anderson Cancer Center, 1515 Holcombe Blvd, Houston, TX 77030. E-mail: sarur@mdanderson.org; and Department of Genetics, Washington University School of Medicine, 660 S. Euclid St. Louis, MO 63110. E-mail: jskeath@genetics.wustl.edu

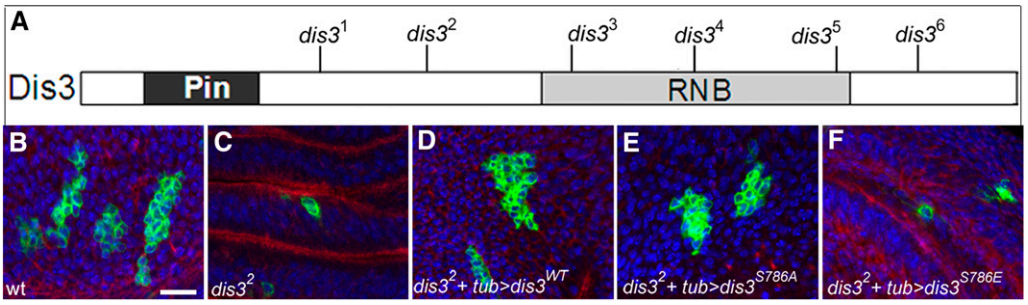

Figure 1 *dis3* is required for cell proliferation. (A) Schematic representation of Dis3 protein showing relevant domains and locations of the six newly generated alleles (black lines). (B–F) Forty-eight-hour-old MARCM clones (green) of indicated genotype in wing discs stained for microfilaments (red) and DNA (blue). (B) Wild type: *hsflp*, *UAS-GFP*, *tub-gal4/+*; *FRT82B tub-gal80/FRT82b dis3²*. (C) *dis3²*: *hsflp*, *UAS-GFP*, *tub-gal4/+*; *FRT82B tub-gal80/FRT82b dis3²*. (D) *dis3²* + *tub* > *dis3^WT*: *UAS-dis3^WT/hsflp*, *UAS-GFP*, *tub-gal4*; *FRT82B tub-gal80/FRT82B dis3²*. (E) *dis3²* + *tub* > *dis3^S786A*. (F) *dis3²* + *tub* > *dis3^S786E* are identical to *dis3²* + *tub* > *dis3^WT* except that *dis3^S786A* and *dis3^S786E* take the place of *dis3^WT*. Bar, 50 μm in B (A) The molecular nature of the *dis3* alleles is as follows: *dis3¹* (C866T and Q252X), *dis3²* (G1255A and W360X), *dis3³* (C1624T and C483X), *dis3⁴* (T2043A and L623X), *dis3⁵* (C2591T and P787L), and *dis3⁶* (G2861A; disrupts splice site at amino acid 858).

reduction of Dis3 exonuclease function retards cell growth; elimination of Dis3 function appears incompatible with cell growth (Tomecki *et al.* 2014). Except for the observation that RNAi-mediated depletion of *dis3* function leads to early larval arrest and reduces tissue growth in *Drosophila* (Hou *et al.* 2012; Towler *et al.*, 2015), the role of *dis3* has not been rigorously explored in higher eukaryotic model systems.

Two other genes—*dis1* and *dis2*—were identified alongside *dis3* in the genetic screen in *S. pombe* for sister chromatid segregation defects (Ohkura *et al.* 1988). *dis1* encodes the founding member of the TOG1/XMAP215 family of microtubule-associated proteins (Nabeshima *et al.* 1995). *dis2* encodes a catalytic subunit of type I protein phosphatases (PP1) (Ohkura *et al.* 1989). In yeast and flies, loss-of-function mutations in *dis1* (*mini-spindles* in flies) and *dis2* (*PP1-87b* in flies) lead to overcondensed chromosomes that distribute unequally among daughter cells at mitosis and result ultimately in a failure or block in mitosis (Ohkura *et al.* 1988; Axton *et al.* 1990; Cullen *et al.* 1999).

In contrast, other studies hint that reduction of *dis2* or *dis3* activity may, in certain contexts, enhance cell division. In cycling *Xenopus* embryo extracts, pharmacological inhibition of PP1 activity triggers premature mitotic entry (Walker *et al.* 1992). In multiple myeloma, a malignancy of plasma B cells, whole genome sequencing approaches uncover *dis3* as one of the most frequently mutated genes in this cancer (Chapman *et al.* 2011; Walker *et al.* 2012; Lohr *et al.* 2014). Essentially all multiple myeloma-specific *dis3* mutations are missense mutations that cluster in its RNB domain and appear to reduce but not eliminate *dis3* function in the tumor cells: *dis3* mutations that are associated with loss of heterozygosity appear to simply reduce Dis3 exonuclease activity, whereas those mutations found associated with a wild-type copy of *dis3* in the tumor appear to largely eliminate exonuclease activity for the variant allele product (Chapman *et al.* 2011; Walker *et al.* 2012; Lohr *et al.* 2014; Tomecki *et al.* 2014). Within multiple myeloma tumors, *dis3* mutations have been found simultaneously clonal with activating mutations in *k-ras* (Lohr *et al.* 2014). However, no direct experimental evidence has linked loss or reduction of *dis3* function to enhanced cell proliferation.

The Ras–ERK pathway drives cells through the G1–S cell cycle transition, by promoting cell growth (Prober and Edgar 2000), and cyclin-dependent kinase I (CDK1), the master regulator of mitosis, triggers mitosis and its associated events via the concerted phosphorylation of a battery of downstream targets (Nigg 2001). But on its own, activation of the Ras–ERK pathway is insufficient to deregulate cell proliferation: in otherwise normal cells, constitutive ras activation, via forced expression of *ras^V12*, an activated form of *ras*, drives cell growth, accelerating cells through G1–S, but leaves cell-doubling times relatively unchanged, resulting in enlarged cells that stack up in the G2 phase of the cell cycle (Prober and Edgar 2000). Except for the trend in multiple myeloma for mutations in *dis3* to co-occur with activating mutations in *k-ras*, no genetic interaction has been found between *dis3* and the Ras–ERK pathway.

Beginning with the *Drosophila* system, we find that the ablation of *dis3* activity or specifically of *dis3*'s exonuclease activity is incompatible with cell division, leading to a variety of mitotic defects. Conversely, we find that reduction of *dis3* activity can enhance cell proliferation when paired with elevated *ras* activity. Extending our findings through the use of the worm and mouse systems, we find that the *ras–dis3* genetic interaction is evolutionarily conserved, and that *dis3* reduction can, in the presence of growth-stimulating conditions, enhance the proliferation of murine B cells, the relevant cancerous cell type in multiple myeloma.

Materials and Methods

Fly strains and transgenes

Wild type is *w1118*. The following stocks were provided by the Bloomington *Drosophila* Stock Center: *UAS-Ras^v12*, *UAS-Ras^DN*, *UAS-Ras^WT*, *UAS-Raf^F179*, *UAS-Raf^DN*, *grk³*, *dis3^P*, *sbr RNAi* (HMS02414), *3L3R FRT* (*w[1118];P{w[+mW.hs]=FRT(w[hs])}2A P{ry[+t7.2]=neoFRT}82B*), *tubP-gal4* (III), *act5C gal4* (II), *MS1096-GAL4*, and *Df(3R)BSC638* and the FUCCI reporter *w*; *Kr^If-1/CyO*; *UAS-CFP.E2f UAS-Venus.NLS.CycB/TM6B Tb*. *dis3 RNAi* (KK101473) and *rop-1 RNAi* (KK104790) were obtained from the Vienna *Drosophila*

Resource Center. The *grk*^{2B} line was provided by Paul Macdonald and *dpp-gal4*, *UAS-GFP*, and *MARCM 82B* (*hsflp*, *UAS GFP*; *tubP-gal4*; *FRT 82B tub gal80/SM6a-TM6b*), by Greg Longmore.

Rescue experiments were carried out using the GAL4/UAS system (Brand and Perrimon 1993). *dis3* alleles were isolated by EMS mutagenesis of *3L3R* flies and screened for lines that failed to complement the *dis3* deficiency, *Df(3R)BSC638*. A complementation group containing *dis3* alleles was identified and sequencing identified the causative lesion in each *dis3* allele (see Figure 1 legend). Mosaic analysis with a repressible cell marker (MARCM) clones were generated by heat shocking larvae for 1 hr at 37° and fixing wing discs from wandering third instar larvae after 48 hr. *dis3*^{P} is an enhancer/promoter (EP) element insertion (Rorth 1996) that contains the GAL4 responsive UAS sequences in its 5′ UTR, and which can be used to drive *dis3* expression under GAL4 control. *Actin-GAL4* mediated expression of *dis3* in flies transheterozygous for *dis3*^{P} and *Df(3R)BSC638*, *dis3*^{1}, or *dis3*^{2} rescue the observed overgrowth phenotype of posterior follicle cells. The chromosome carrying *dis3*^{P} is homozygous lethal, but *dis3*^{G5039} over *Df(3R)BSC638* is viable. Thus, the *dis3*^{P} chromosome appears to carry an associated lethal mutation.

UAS transgenes were generated by amplifying region 6–3066 of the *dis3* cDNA, SD10981 (accession AY052150.1) and directionally cloning into the *Not*I and *Xba*I sites of pUASp-ATT (Becalska and Gavis 2010). PCR-based mutagenesis was used to create phosphomimetic S786E (TCG > GAG) and non-phosphorylateable S786A (TCG > GCC) forms of the *dis3* transgene. *dis3* transgenes were inserted into the attp40 landing site on 2L (Genetic Services).

Antibody production, immunostaining, and neuroblast squashes

The N-terminal 500 amino acids of Dis3 were expressed as a his-tagged fusion protein, purified, and used to immunize guinea pigs and rabbits (Pocono Rabbit Farm and Laboratory). Purified Dis3 fusion protein was cross-linked to cyanogen bromide sepharose resin and used for affinity purification of anti-Dis3 antibodies as described in Arur and Schedl (2014). For immunostaining, tissues were dissected in PBS, fixed in 3.7% formaldehyde in PBS, washed in PBS 0.1% Tween, blocked with 1% BSA in PBS 0.1% Tween, and incubated with primary antibodies and Alexa-Fluor-conjugated secondary antibodies (Life Technologies). Immunofluorescence was performed as described using the following antibodies: rabbit anti-dpERK (Cell Signaling), guinea pig anti-Dpn (1/1000), mouse anti-tubulin (1/50, E7, Developmental Studies Hybridoma Bank), and rabbit antiphospho-(Ser10)-histone 3 (1:4000). DAPI and rhodamine phalloidin were used to stain DNA and microfilaments.

Orcein staining of third instar larval neuroblasts was performed as in Fanti and Pimpinelli (2004). The degree of chromosome condensation was scored in hypotonically treated brains, while aneuploidy was scored in hypotonic- and colchicine-treated brains.

Table 1 Dis3 function is required for cell division

Genotype of MARCM clones	Cells/clone	*n*
WT	18.8 ± 8.8	15
dis3^{1}	2.0 ± 1.1	17
dis3^{2}	1.9 ± 0.8	15
dis3^{2} + *tub* > *dis3*^{WT}	17.2 ± 12.0	22
dis3^{2} + *tub* > *dis3*^{S786A}	16.8 ± 9.4	12
dis3^{2} + *tub* > *dis3*^{S786E}	3.4 ± 2.1	24
dis3^{2} + *tub* > *P35*	2.6 ± 1.3	31

wt, FRT2A, FRT82D; ±, standard deviation.

Measurements of imaginal disc area were performed by selecting wandering third instar larvae with everted spiracles, sorting for sex, and fixing imaginal discs via standard methods. Area measurements were performed using ImageJ. We note that imaginal discs that coexpressed *dis3* RNAi and *ras*^{v12} transgenes exhibited increased folding relative to all other genotypes; thus measurements of tissue size in this background likely underestimate the effect of *dis3* and *ras*^{v12} on tissue growth and size.

Exonucleolytic and encoducleolytic RNA assays

Dis3 RNA exonuclease assays were adapted from Mamolen *et al.* (2011) and performed in quadruplicate. Maltose binding protein (MBP) or N-terminal MBP fusions of full-length Dis3, Dis3^{S786A} (TCG > GCC), Dis3^{S786E} (TCG > GAG), and Dis3^{P787L} (CCC > CTC) were expressed in *Escherichia coli* and purified on amylose resin. A 96-nt RNA substrate was generated by T7 transcription of *Not*I digested pBS SK. Purified proteins were diluted to 60 nM concentration in 10 mM Tris, pH 8.0, 75 mM KCl, and 40 μM MgCl2 containing 3 ng/μl RNA. This mix was incubated at 37° until the indicated time points before aliquots were taken and added to formamide loading buffer. RNAs were run on 2% agarose gels before visualization. Quantitation was performed using ImageJ.

Dis3 RNA endonuclease assays were performed in quadruplicate essentially as described in Lebreton *et al.* (2008). Briefly, to generate a circular RNA substrate, a 461-nt fragment was PCR amplified with T7 promoter on the 5′ end and SP6 promoter on the 3′ end. The PCR product was gel purified, and 1 μg of purified DNA template was used in an *in vitro* transcription reaction with T7 RNA polymerase. The *in vitro* transcription reaction was performed for 1 hr at 37°. At the end of the reaction, 10 units of DNAseI treatment was performed to eliminate the DNA template, and the single-strand RNA was purified via standard methods. A total of 5 μg of linear purified RNA was then treated with 1 unit of T4 RNA ligase, 10% PEG, and 100 nM ATP in 1× ligase buffer overnight at 15°. The circular RNA was then gel purified and eluted in DEPC water. The RNA was quantified by spectrophotometer before analysis. Each experimental replicate was performed using freshly generated and circularized single-strand RNA.

To assess the endonuclease assay of each form of Dis3, purified proteins were diluted to 60 nM concentration in 10 mM Tri, pH 8.0, 75 mM KCl, and 40 μM MnCl2 containing about 4 μg/μl circularized RNA. This mix was incubated at

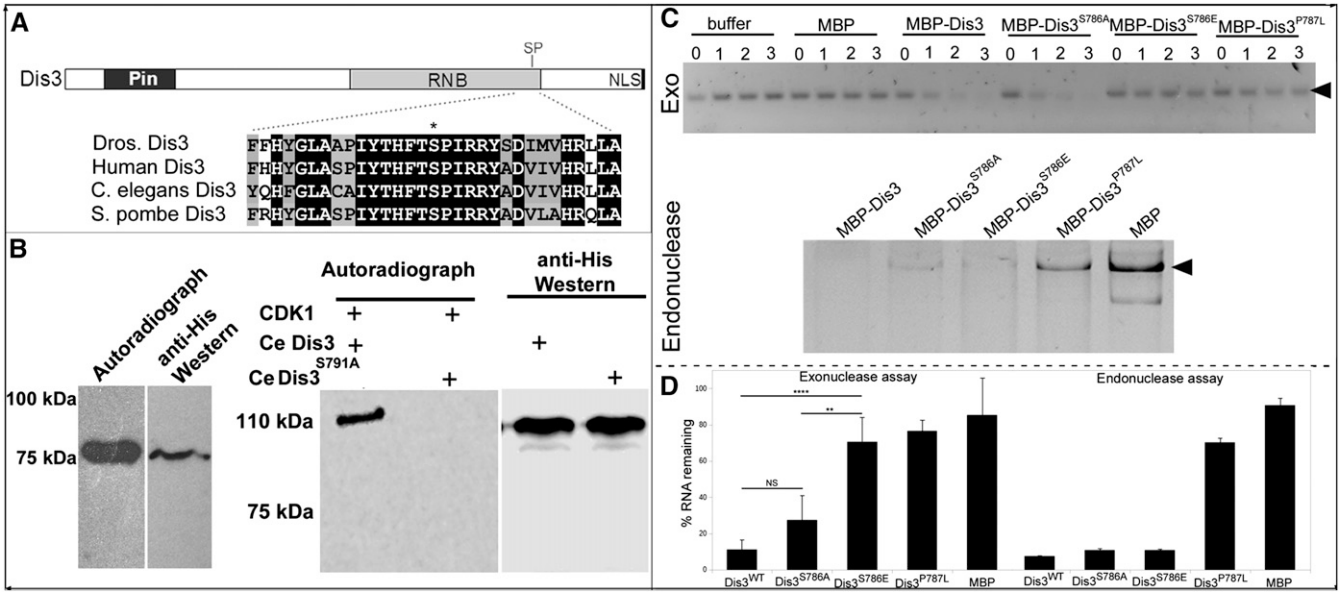

Figure 2 CDK1 phosphorylates Dis3 *in vitro* and inhibits its exonuclease activity. (A) Schematic representation of Dis3 with relevant protein domains indicated. Alignment of a portion of the catalytic region of Dis3's RNA exonuclease domain with the predicted CDK1 phosphorylation site (SP) marked by *. (B) *In vitro* kinase assays showing that CDK1 phosphorylates a 75-kDa C-terminal form of *Drosophila* Dis3 (left) and a full-length 110-kDa form of *C. elegans* Dis3^{WT} but not Dis3^{S791A} (right); in both panels, the anti-His Western blot shows protein loading of the 75-kDa C-terminal form of *Drosophila* Dis3, and the 110-kDa full-length forms of *C. elegans* Dis3. All assays were repeated at least three times. (C, top) Exonuclease activity of indicated forms of full-length *Drosophila* Dis3 acting on a 96-bp RNA substrate (arrowhead) as a function of time (in hours). Exonuclease assays were performed in the presence of buffer alone, maltose binding protein (MBP), or MBP fusions of the indicated forms of Dis3. (Bottom) Endonuclease activity of indicated forms of Dis3 acting on a circular 461-bp RNA molecule (arrowhead). (D) A graph quantifying three independent exonuclease assays and four independent endonuclease assays (bottom). Error bars indicate 95% confidence intervals. ** $P < 0.01$; **** $P < 0.0001$.

37° for 1 hr before aliquots were taken and added to formamide loading buffer. RNAs were run on 7% native polyacrylamide gels before visualization. Quantitation was performed using a spectrophotometer.

In vitro CDK1 kinase assays and mass spectrometry analysis

Recombinant 6× HIS-tagged wild-type *Drosophila* Dis3 protein was made by cloning a PCR product corresponding to amino acids 451–982 of the wild-type protein into the pTrcHis Topo vector (cat. no. K4410-01). Recombinant 6× HIS-tagged, full-length forms of *Caenorhabditis elegans* Dis3^{WT} and Dis3^{S791A} were created in a similar manner. Clones were verified by sequencing for orientation and sequence integrity. Proteins were expressed using BL21(DE3) (Sigma) cells, at 20° using 1 mM isopropyl β-D-1-thiogalactopyranoside for 16 hr. Proteins were purified using Ni-NTA agarose or glutathione sepharose. The amount of purified protein was estimated by conducting bicinchoninic acid assay (BCA)-based protein assays and comparing band intensities of purified protein samples with BSA dilution series standards on a Coomassie-stained gel following 10% SDS–PAGE.

In vitro kinase assays were carried out as described previously (Arur *et al.* 2009) using purified CDK1/cyclinA2 kinase (Promega; V2961). Briefly, for each protein, a standard 25-μl reaction containing 100 ng of purified protein, 50 μM cold ATP, and 1 μM [^{32}P]γATP (6000 Ci/mmol; PerkinElmer) was performed. SDS–PAGE and autoradiography were used to establish that the intact fusion protein contained most of the incorporated ^{32}P.

The paired *in vitro* kinase assays and phosphopeptide analysis were performed as detailed above with the following modifications. A standard 25-μl reaction contained 500 ng of purified protein, 100 μM cold ATP (Sigma), 1× kinase buffer, and 5 units of active CDK1/cyclinA2 enzyme. Reactions were terminated after 15 min at 30°, at which time ATP incorporation was linear with respect to time. The phosphorylated protein was bound to an Ni-NTA column and washed with 1× kinase buffer. The protein was then eluted with 100 μl 250 mM imidazole and dialyzed into PBS overnight at 4°. The dialyzed protein was shipped to the Harvard University's Taplin Biological Mass Spectrometry Facility for phosphopeptide analysis.

Image acquisition and preparation details

Imaging of orcein-stained neuroblasts was performed at room temperature on a Zeiss axioplan 2 microscope fitted with an Olympus DP71 camera using a ×63 apochromat oil immersion lens with a numerical aperature (N.A.) of 1.4. DP image acquisition software was used to acquire images. All other imaging was performed on a Zeiss LSM700 confocal microscope using ×63 apochromat oil immersion (N.A. 1.4), ×40 Neofluor oil immersion (N.A. 1.3), and ×10 Neofluor air (N.A. 0.3) lenses. Tissue was mounted in 70% glycerol containing 0.3× PBS and 2% propyl gallate. Images were acquired using ZEN 2009 software (Zeiss) exported as TIFF images and brightness and contrast were adjusted using Adobe

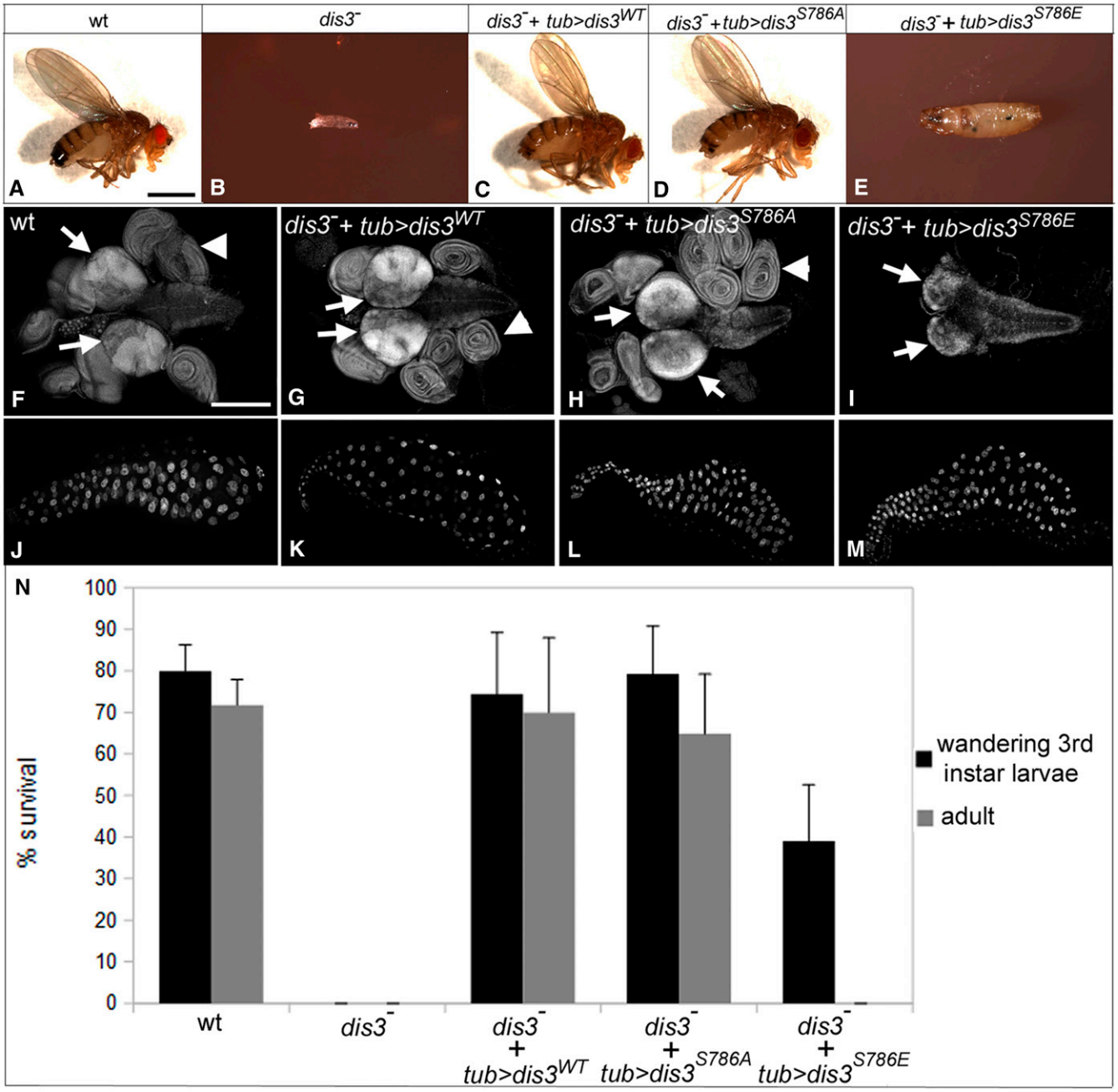

Figure 3 Dis3 phosphorylation inhibits Dis3 function *in vivo*. (A–E) Terminal phenotype of flies of indicated genotype. (F–I) Images of the larval brain/CNS (arrows) and imaginal disc complexes (arrowheads) and (J–M) salivary glands from third instar larvae of indicated genotype. (N) Graph of percent survival of flies of indicated genotype to wandering late third instar stage (black) or adulthood (gray). In A–I, wild type: FRT2A FRT82B; $dis3^{-}$: $dis3^{1}/dis3^{2}$; $dis3^{-}$ + *tub* > $dis3^{WT}$: *UAS-dis3*^{WT}/+; *tub-gal4* $dis3^{1}/dis3^{2}$; $dis3^{-}$ + *tub* > $dis3^{S786A}$: *UAS-dis3*^{S786A}/+, *tub-gal4* $dis3^{1}/dis3^{2}$; and $dis3^{-}$ + *tub* > $dis3^{S786E}$: *UAS-dis3*^{S786E}/+; *tub-gal4* $dis3^{1}/dis3^{2}$. Error bars indicate 95% confidence intervals. Bars, 1 mm in A–E and 200 μm in F–M.

Photoshop. All images are single confocal slices except Figure 4C, which is a maximum projection of a confocal *Z*-stack (performed using ZEN 2009 software).

RNAi-interference experiments in the C. elegans germ line

A *dis-3* RNAi clone was generated by amplification of 1 kb of the open reading frame starting from ATG and inserted into the pPD129.36 RNAi vector. The clone was sequence verified before analysis. When adult *C. elegans* were grown on *dis-3* RNAi plates, the resulting progeny died during early larval stages. Thus RNAi analysis was performed with L1 larvae grown on RNAi plates and analyzed 24 hr past the L4 larval stage. All RNAi experiments were performed in the *rrf-1* background. RRF-1 is a soma-specific RNA-dependent RNA polymerase that is necessary for the RISC complex to function

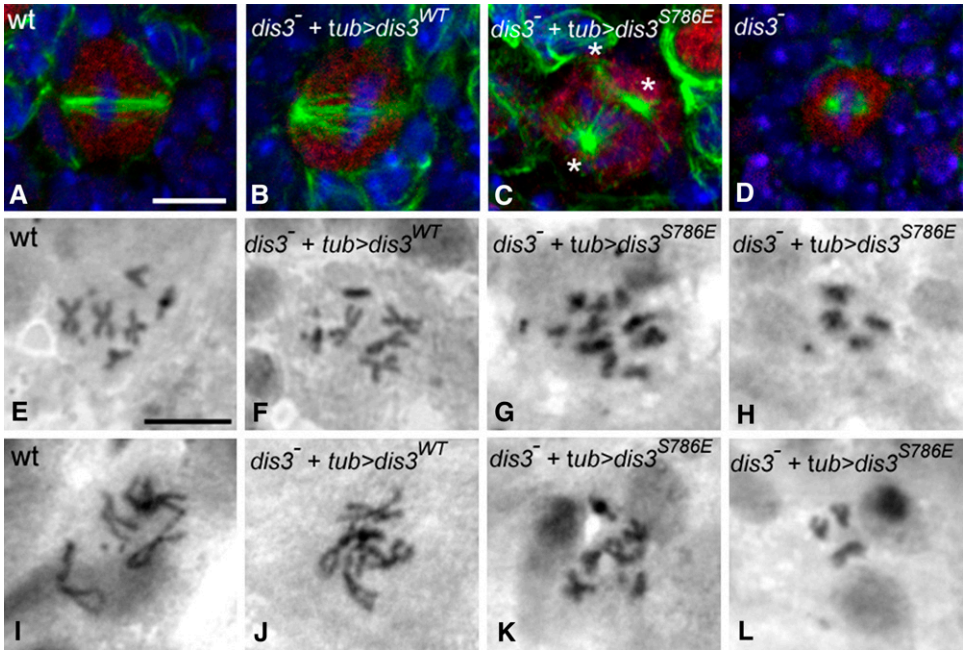

Figure 4 Loss of Dis3 exonuclease activity causes mitotic defects and excessive chromosome condensation. (A–D) Larvae of the indicated genotype labeled for neuroblasts (red), microtubules (green), and DNA (blue). (C) Inhibition of Dis3 exonuclease activity induces mitotic defects, such as multipolar spindles: * indicates three microtubule organizing centers. (D) *dis3*$^{1/2}$ larvae possess shortened mitotic spindles. (E–L) Orcein staining of chromosomes in (E–H) hypotonic- and colchicine-treated or (I–L) only hypotonic-treated neuroblasts of indicated genotypes. Genotypes are as detailed in Figure 3. Bar, 5 μm.

in the soma. In the absence of *rrf-1*, RNAi is elicited in the germ line but not in most somatic tissues, thus the function of genes can be assayed during adult germ line development.

Mouse strains

All experiments involving animals were performed according to protocols approved by the Washington University School of Medicine Animal Studies Committee. C57BL/KalwRij *AID-Cre;LSL-Kras*$^{G12D/+}$ and *AID-Cre;LSL-Kras*$^{+/+}$ transgenic mice were generated by backcrossing *AID-Cre* knock-in mice and *LSL-Kras*^{G12D} mice onto the C57BL/KaLwRij background for at least 10 generations, then breeding the backcrossed strains together. The *ROSA*26-EYFP allele was removed from *AID-Cre* mice over the course of backcrossing. For genotyping, DNA was isolated from tail snips using DNeasy Blood and Tissue kit (Qiagen).

Plasmid constructs

Lentiviral pLKO.1-puro vectors containing short hairpin RNAs (shRNAs) targeting murine *Dis3* (RNAi Consortium clone IDs: TRCN0000120742 and TRCN0000120744, referred to as sh*Dis3*0.1 and sh*Dis3*0.2, respectively) were purchased from Sigma-Aldrich.

Viral production and transduction experiments

Recombinant lentiviruses were produced by transient cotransfection of 293T cells with shRNA constructs along with packaging plasmid psPAX2 and envelope plasmid pMD2.G using Lipofectamine 3000 (Invitrogen). Viral supernatants were harvested 48 hr post-transfection and concentrated using Retro-X Concentrator (Clontech). Titers were determined by transducing NIH/3T3 cells with serial dilutions of concentrated supernatant and selecting with puromycin. All transduction experiments were performed in the presence of 10 μg/ml polybrene.

Murine B cell growth assay

Spleens were harvested from mice and single-cell suspensions generated by passing tissue through 70-μm cell strainers (Corning). Red blood cells were removed by brief treatment with hypotonic lysis buffer (Sigma-Aldrich). Splenocytes were washed once in staining buffer (0.5% BSA and 2 mM EDTA in PBS), then naive B cells were isolated by immunomagnetic depletion using anti-CD43 microbeads and LD columns (Miltenyi Biotec). CD43$^-$ B cells were then cultured for 24 hr in stimulation media consisting of RPMI 1640 media (ATCC), 10% FBS (Hyclone), 50 μM β-mercaptoethanol (Sigma-Aldrich), 1% penicillin–streptomycin (Corning), 10 μg/ml LPS (Sigma-Aldrich), and 20 ng/ml IL-4 (R&D Systems), before transduction with lentiviral shRNAs. Transduced B cells were plated at 50,000 cells in 400 μl of stimulation media per well of 48-well plates (day 0). Cell numbers were then assessed on successive days using a Neubauer hemocytometer and Trypan blue staining.

RNA isolation and quantitative real-time PCR

RNA was isolated using the RNeasy Plus or miRNeasy kit (Qiagen) and quantified on an H4 Synergy microplate reader (Biotek). RNA was then reverse transcribed with iScript RT Supermix (Bio-Rad). cDNA input was standardized and quantitative PCR (qPCR) reactions were performed with Taqman Fast Advanced Master Mix (Applied Biosystems). Taqman probes (Applied Biosystems) were as follows: *Dis3* (Mm01224318_m1), *Actb* (Mm00607939_s1), *18S* (Mm03928990_g1), and *Ywhaz* (Mm01158416_g1). All real-time (RT)-qPCR reactions were performed on a CFX96 Connect Real-Time PCR System (Bio-Rad). Target gene expression levels were normalized to averaged *Actb*, *18S*, and *Ywhaz* expression levels and fold change was determined with the ddCt method.

Table 2 Dis3 RNA exonuclease activity is required for normal mitosis

Genotype	Aneuploidy (*n*)	Overcondensed chromosomes (*n*)	Mitotic index (*n*)
Wild-type	0% (820)	0% (450)	14.1% (265/1878)
$dis3^{-}$ + $dis3^{wta}$	0.1% (1/927)	0.5% (2/414)	20.9% (280/1337)
$dis3^{-}$ + $dis3^{S786Eb}$	5.0% (8/160)	44.0% (73/166)	26.8% (398/1484)
$dis3^{-}$ + $dis3^{S786A}$	0.2% (2/819)	1.3% (6/463)	18.8% (314/1671)
	$P < 1 \times 10^{-5c}$	$P < 0.1 \times 10^{-10c}$	$^{d}P < 0.0005$

[a] $dis3^{1/2}$ mutant larvae that express the wild-type *dis3* transgene.
[b] $dis3^{1/2}$ mutant larvae that express the phosphomimetic *dis3* transgene.
[c] Fisher's exact test: comparing $dis3^{-}$ + $dis3^{wt}$ to $dis3^{-}$ + $dis3^{S786E}$.
[d] Chi-square test: comparing $dis3^{-}$ + $dis3^{wt}$ to $dis3^{-}$ + $dis3^{S786E}$.

SDS–PAGE and immunoblotting

Cells were lysed in ice-cold 1× RIPA lysis buffer (Millipore, 50 mM Tris-HCl, pH 7.4, 150 mM NaCl, 0.25% deoxycholic acid, 1% NP-40, 1 mM EDTA), containing 1× Halt Protease and Phosphatase Inhibitor Cocktail (Pierce) on ice for 30 min. Lysates were clarified by centrifugation and protein content measured using the BCA Protein Assay kit (Pierce). A total of 40 μg of protein was resolved on 4–20% TGX gels (Bio-Rad) and transferred onto PVDF membranes (Bio-Rad). Membranes were blocked in Tris-buffered saline containing 0.1% Tween 20 (TBST) with 5% BSA added, before incubation overnight at 4° with primary antibodies against DIS3 (Proteintech). The membranes were then washed with TBST and incubated with the appropriate horseradish peroxidase (HRP)-conjugated secondary antibody for 1 hr at room temperature. Results were visualized with SuperSignal West Dura Extended Duration Substrate (Pierce) and imaged on a ChemiDoc XRS system (Bio-Rad).

Data availability

The authors state that all data necessary for confirming the conclusions presented in the article are represented fully within the article.

Results

Abrogation of Dis3 activity is incompatible with cell division

To discern the null phenotype of *dis3* in flies, we used an EMS-based noncomplementation screen to generate six new *dis3* alleles: $dis3^{1}$–$dis3^{6}$, four of which encode premature stop codons (Figure 1A and legend). All six alleles are homozygous lethal and exhibit indistinguishable phenotypes in *trans* to each other or a deficiency of the region—larvae reach the second larval instar stage, persist at this stage for up to 8 days, and die, similar to what has been observed for RNAi-mediated depletion of *dis3* function (Hou *et al.* 2012; Towler *et al.*, 2015). All six alleles then behave like null or strong hypomorphic alleles of *dis3*, and *dis3* is an essential gene with its maternal stores apparently sufficient to direct embryonic and larval development to the second larval instar stage.

To assess the effect of ablation of *dis3* function on cell division, we used the MARCM system to induce mitotic cell clones homozygous mutant for $dis3^{1}$ or $dis3^{2}$, the two *dis3* alleles with the earliest premature stop codons, in second instar larvae, and counted the number of cells per clone 48 hr later (Figure 1, B–E; Table 1). Control wild-type clones contained 18.8 ± 8.8 cells per clone, while $dis3^{1}$ or $dis3^{2}$ mutant clones contained 2.0 ± 1.1 or 1.9 ± 0.8 cells per clone, respectively, with this phenotype fully rescued by expression of a wild-type *dis3* transgene. Apoptosis does not account for the small size of *dis3* mutant clones, as expression of the baculovirus cell death inhibitor P35 did not increase cell number of *dis3* mutant clones (Table 1). During the 48-hr time window, wild-type cells then underwent on average four cell doublings, and cells homozygous mutant for $dis3^{1}$ or $dis3^{2}$ underwent one cell doubling. Based on the maternal perdurance of *dis3* gene function, we infer that perdurance of Dis3 protein within mutant clones allows for one cell division and that abrogation of *dis3* function inhibits or blocks cell growth and/or division.

CDK1-mediated phosphorylation of Dis3 inhibits its exonuclease activity

dis3 was initially identified alongside *dis1* and *dis2* in a screen for sister chromatid segregation defects in *S. pombe* (Ohkura *et al.* 1988). *dis1* encodes a TOG1/XMAP215 family of microtubule-associated proteins; *dis2* encodes a catalytic subunit of type I protein phosphatases (PP1) (Ohkura *et al.* 1989; Nabeshima *et al.* 1995). In yeast and mammalian cells, loss-of-function mutations in *dis1* and *dis2* delay or block mitosis (Ohkura *et al.* 1988; Fernandez *et al.* 1992; Gergely *et al.* 2003), phenotypes similar to what we observed for *dis3*. Dis1 and Dis2 are also phosphorylated by CDK1 during mitosis and localize to the centromere (Yamano *et al.* 1994; Nabeshima *et al.* 1995; Kwon *et al.* 1997; Trinkle-Mulcahy *et al.* 2003; *Aoki et al.* 2006). Thus, we asked whether CDK1 can phosphorylate Dis3. Dis3 contains a conserved, consensus CDK1 phosphorylation sites (S/T-P-x-K/R), S786 in flies, nestled within a stretch of 12 amino acids within the exonuclease active site perfectly conserved between yeast and humans (Figure 2A). Using a purified, C-terminal form of wild-type *Drosophila* Dis3, we combined *in vitro* kinase assays, mass spectrometry analysis, and phosphopeptide analysis to identify S786 as the major site phosphorylated by active CDK1:cyclinA2, with 18.2% of total peptides containing phospho-S786 (Figure 2B; Supplemental Material, Figure

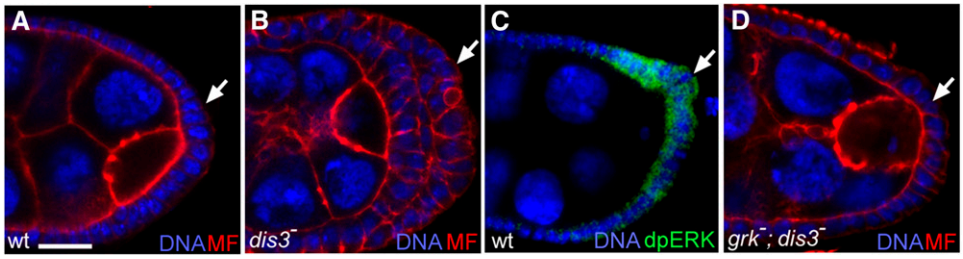

Figure 5 Reduction of Dis3 function promotes tissue growth. (A–D) High magnification views of the posterior portion of *Drosophila* egg chambers from wild-type (A and C), *dis3^{P}/Df(3R) BSC638* mutant (B), and *grk^{2B}/grk^{3}; dis3^{P}/dis3^{2}* mutant (D) females stained for DNA (blue; B–E), microfilaments (red; A, B, and D), and dpERK (green; C). Arrows point to posterior follicle cells. Bar, 10 μm.

S1). Similar *in vitro* kinase assays verified that CDK1 phosphorylates *C. elegans* Dis3 on the cognate phosphorylation site (S791; Figure 2B). Thus, the ability of CDK1 to phosphorylate Dis3 in its exonuclease domain appears conserved evolutionarily.

Next, we assessed the effect of phosphorylation on Dis3 exonuclease and endonuclease activity *in vitro*, using four full-length, recombinant forms of Dis3, each fused N-terminally to maltose binding protein—a wild-type form, a nonphosphorylatable form in which we mutated S786 to A, a phosphomimetic form in which we mutated S786 to E, and a form that contained the Dis3 P787L mutation (the mutation in *dis3^{5}*) in the phosphoacceptor site of Dis3 (Figure 2C). To measure exonuclease activity, we assayed the ability of each form of Dis3 to degrade a linear 96-nucleotide RNA molecule in the presence of Mg^{++}, which is required for optimal exonuclease activity, but not Mn^{++}, which is required for optimal endonuclease activity (Schaeffer *et al.* 2009). To measure endonuclease activity, which is encoded by the N-terminal PIN domain, we assayed the ability of each form of Dis3 to degrade a circular 461-nucleotide RNA molecule in the presence of Mn^{++}, but not Mg^{++}. The wild-type and nonphosphorylatable forms of Dis3 possessed significant RNA exonuclease activity, but the phosphomimetic and P787L forms largely lacked such activity (Figure 2, C and D). In contrast, all Dis3 forms except Dis3^{P787L} retained significant RNA endonuclease activity (Figure 2, C and D). We infer that CDK1-mediated phosphorylation of Dis3 on S786 inhibits its RNA exonuclease, but not endonuclease, activity and that the P787L mutations alter both activities, likely because it disrupts overall protein structure.

Next, we sought to test the specific functional requirement of Dis3's exonuclease activity *in vivo*. Here, we generated three UAS-linked *dis3* transgenes (wild type, nonphosphorylatable, and phosphomimetic) and assessed the ability of each to rescue the lack of cell division observed in *dis3* mutant MARCM clones and the larval lethal phenotype of flies that lack zygotic *dis3* function. Expression of the wild-type or nonphosphorylatable, but not the phosphomimetic, *dis3* transgene rescued the cell division phenotype of *dis3* mutant clones (Figure 1, D–F; Table 1; see Figure S1 for relative expression of each transgene). Likewise, ubiquitous expression of the wild-type or nonphosphorylatable *dis3* transgene rescued the lethal phenotype of *dis3$^{1/2}$* larvae, producing morphologically normal adult flies at normal developmental timing (Figure 3, A–D and N). Expression of the phosphomimetic *dis3* transgene in the *dis3$^{1/2}$* mutant background rescued larval development to the late wandering third larval instar stage, but larvae took 7–12 extra days to reach this stage and died at or shortly after it (Figure 3, E and N). Dissection of these larvae revealed that their imaginal tissues, which grow via mitotic cell cycles, were either lacking (imaginal discs) or reduced in size (brains and ventral nerve cord) (compare Figure 3I to Figure 3, F–H), but that their larval tissues, such as salivary glands, which grow via endoreduplication, were of grossly normal size and morphology (compare Figure 3M to Figure 3, J–L). This phenotypic syndrome in which late larval/early pupal lethality is coupled to missing imaginal discs and reduced central nervous system size, but normal larval structures, is characteristic of mutations in essential mitotic functions (Gatti and Baker 1989). The ability of the phosphomimetic *dis3* transgene to rescue endocycles and larval development, at least to late larval stages, but its inability to rescue the mitotic cell division and the growth of imaginal tissues, strongly support a model for a mitotic function of Dis3's exonuclease activity.

Inhibition of Dis3 exonuclease activity leads to mitotic defects

The apparent defects in the mitotic cell cycle in larvae that lack *dis3*'s exonuclease function led us to examine the role of *dis3* exonuclease activity in mitosis. Initially, we assessed the morphology of the mitotic spindle in dividing neuroblasts of wild-type third instar larvae and of third instar larvae homozygous mutant for *dis3* that expressed the wild-type, nonphosphorylatable, or phosphomimetic *dis3* transgene under the control of *Tubulin-GAL4*. All mitotic neuroblasts in wild-type ($n = 30$) or *dis3* mutant larvae rescued by the wild-type *dis3* transgene ($n = 24$) and all but one in *dis3* mutant larvae rescued by the nonphosphorylatable transgene ($n = 44$) displayed normal mitotic spindles that spanned essentially the full width of the cell (Figure 4, A and B). In contrast, in *dis3* mutant larvae rescued by the phosphomimetic transgene, 24% of mitotic neuroblasts ($n = 8/34$) exhibited defective mitotic spindles that were multipolar (12%; Figure 4C), disorganized (9%), or short (3%). Mitotic spindles were also shorter in *dis3$^{1/2}$* mutant larvae, than in wild type (4.2 μm *vs.* 5.4 μm; $n = 13$; $P < 0.003$) and failed to span the full width of the cell 70% of the time (Figure 4D). We infer that *dis3* exonuclease activity is required for normal mitotic spindle formation.

Consistent with mitotic defects, using aceto-orcein to stain chromosomes in mitotic neuroblasts in squashed preparations of late third instar larval brains, we found that 5% of mitotic neuroblasts exhibited obvious aneuploidy in *dis3* mutant larvae rescued with the phosphomimetic *dis3* transgene compared to 0%, 0.1%, and 0.2% of mitotic neuroblasts exhibiting this phenotype in wild-type larvae or *dis3* mutant larvae rescued with the wild-type or nonphosphorylatable *dis3* transgene (Table 2; Figure 4, E–H). In addition, 44.0% of mitotic neuroblasts displayed overcondensed chromosomes in *dis3* mutant larvae rescued with the phosphomimetic transgene compared to 0, 0.5, and 1.3% of mitotic neuroblasts exhibiting this phenotype in wild-type larvae or *dis3* mutant larvae rescued with the wild-type or nonphosphorylatable *dis3* transgene (Table 2; Figure 4, I–L). Overcondensed chromosomes are commonly seen when cells are blocked in mitosis, as chromosome condensation occurs during the arrest. Consistent with this, a significantly higher fraction of larval brain neuroblasts labeled positive for the mitotic marker phosphohistone H3 in *dis3* mutant larvae rescued with the phosphomimetic transgene relative to wild-type larvae or *dis3* mutant larvae rescued with the wild-type or nonphosphorylatable transgene (Table 2). The high degree of chromosome condensation and high mitotic index of cells that lack *dis3* exonuclease activity suggest that these cells are blocked or delayed in mitosis and that *dis3*'s exonuclease activity is required for mitotic exit.

Reduction of dis3 activity deregulates proliferation in a Ras–ERK signaling-dependent manner

Elimination of *dis3* function in yeast, flies, and vertebrate cells appears to reduce cell growth and division (Ohkura *et al.* 1988; Kiss and Andrulis 2010; Tomecki *et al.* 2014; and this article), but *de novo*, tumor-specific, apparently hypomorphic mutations in *dis3* are found recurrently in multiple myeloma (Chapman *et al.* 2011; Walker *et al.* 2012; Lohr *et al.* 2014), a cancer of plasma B cells, suggesting that *dis3* promotes progression of this cancer. To explore this possibility, we examined the phenotype of flies transheterozygous for $dis3^{1}$, $dis3^{2}$, or a deficiency of the region and $dis3^{G5039}$, a *P*-element insertion of the P[EP] type (Rorth 1996) in *dis3*'s 5′ UTR, here referred to as $dis3^{P}$. Flies of these genotypes are viable, largely infertile, morphologically normal (except for small bristles and occasional crumpled wings), and exhibit a ~63% reduction in Dis3 protein levels (Figure S2A). Detailed analysis of oogenesis in these flies revealed that 65–74% of stage 5–6 egg chambers displayed excess posterior follicle cells (Figure 5, A and B; Figure S2, B and C; Table 3). Expression of the wild-type *dis3* gene in these *dis3* hypomorphic backgrounds rescued this phenotype (Figure S2D; Table 3). Thus, reduction of *dis3* activity yields excess posterior follicle cells. Loss of epithelial polarity, via mutations in genes such as *discs large*, can cause follicle cell overproliferation (Goode and Perrimon 1997), but follicle cell polarity is grossly normal in these *dis3* hypomorphic backgrounds (Figure S3), suggesting that reduction of *dis3* activity drives overproliferation through a distinct mechanism.

Table 3 Reduction of *dis3* activity induces *ras*-dependent overproliferation in the ovary

Genotype	% egg chambers with posterior overproliferation	*n*
WT	0	100
$dis3^{G5039}/Df(3R)BSC638$	74	68
$dis3^{G5039}/dis3^{1}$	70	46
$dis3^{G5039}/dis3^{2}$	65	101
grk^{2B}/grk^{3}; $dis3^{G5039}/dis3^{2}$	6[a]	94
actin gal4/+; $dis3^{G5039}/dis3^{1}$	0[b]	50

[a] Fisher's exact test: $P < 1 \times 10^{-18}$ comparing grk^{2B}/grk^{3}; $dis3^{G5039}/dis3^{2}$ to $dis3^{G5039}/dis3^{2}$.
[b] Fisher's exact test: $P < 1 \times 10^{-15}$ comparing *actin gal4/+*; $dis3^{G5039}/dis3^{1}$ to $dis3^{G5039}/dis3^{1}$.

During oogenesis, Gurken, an EGF-ligand, signals via the EGF–Ras–ERK pathway to specify posterior follicle cell fate (Neuman-Silberberg and Schüpbach 1993; Nilson and Schüpbach 1999), an event marked by accumulation of the active, diphosphorylated form of ERK in posterior follicle cells (Figure 5C) (Gabay *et al.* 1997). The Ras–ERK pathway promotes cell proliferation in many contexts (*e.g.*, Murphy and Blenis 2006). Thus, we asked whether posterior follicle cell overgrowth in *dis3* hypomorphic backgrounds depended on *gurken* function: Reducing *gurken* function in otherwise $dis3^{P}/dis3^{null}$ flies suppressed follicle cell overgrowth essentially to wild type (Figure 5D; Table 3). The observed overgrowth of follicle cells then requires *gurken* function and that of the Ras–ERK pathway. In *dis3* single mutants, although posterior follicle cell number is increased, the levels of active diphosphorylated ERK in those posterior follicle cells that abut the oocyte, the source of the Gurken signal, appear qualitatively similar (Figure S2, E and F). Thus, *dis3* appears to act downstream of or in parallel to ERK to inhibit the ability of posterior follicle cells to divide in response to Ras–ERK pathway activity.

To test whether attenuating *dis3* activity and elevating Ras–ERK pathway activity can drive tissue overgrowth in other contexts, we used the GAL4/UAS system and the *dpp-GAL4* and *1096-GAL4* driver lines to deplete *dis3* function and/or elevate Ras–ERK activity in restricted sets of cells in developing eye and wing imaginal discs (marked by coactivation of the *UAS-GFP* transgene; Figure 6; Figure S4). To reduce *dis3* function, we drove expression of a UAS-linked *dis3-RNAi* transgene; to elevate Ras–ERK pathway activity, we drove expression of UAS-linked transgenes of ras^{V12} or raf^{F179}—constitutively active forms of *ras* and *raf*. Expression of the *dis3-RNAi* transgene by itself had no gross effect on the size or shape of eye or wing imaginal discs or of the size of GFP^{+} tissue (Figure 6, B and I; Figure S4). Expression of either the ras^{V12} or raf^{F179} transgene led to an increase in the size of GFP^{+} tissue (Figure 6, C, E, and I; Figure S4). Coexpression of the *dis3* RNAi transgene with ras^{V12} or the raf^{F179} elicited a significant increase in the size of GFP^{+} tissue relative to that observed upon expression of ras^{V12} or raf^{F179} alone (Figure 6, D, F, and I; Figure S4). In contrast, coexpression of the *dis3-RNAi* transgene with either wild-type or dominant-negative

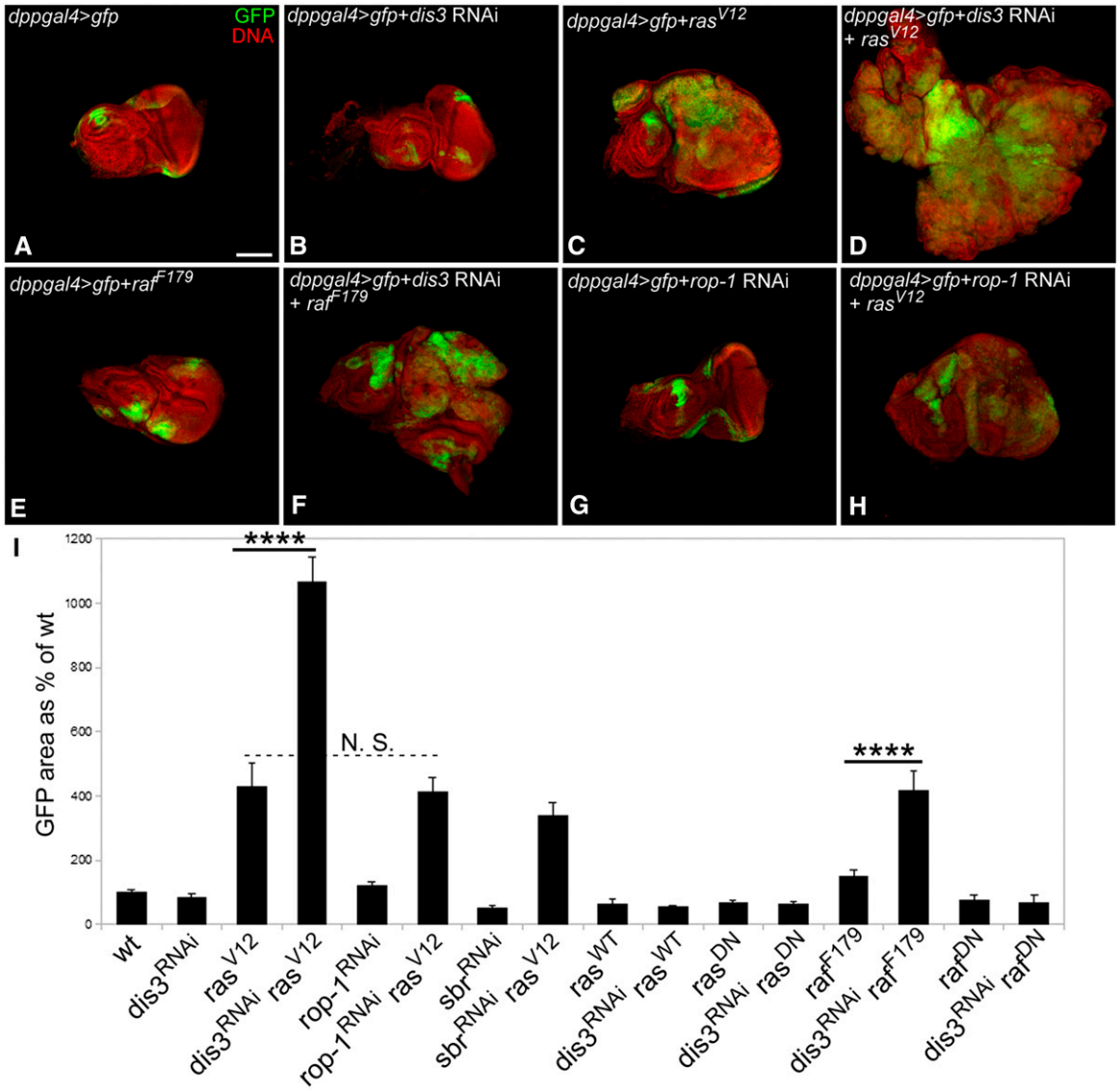

Figure 6 Dis3 and the Ras–ERK pathway genetically interact to drive tissue overgrowth. (A–H) Low magnification views of eye-antennal imaginal discs in which GFP (green) and the indicated UAS-linked transgenes (*e.g.*, *dis3*^{RNAi}) were driven under the control of *dpp-GAL4*. DNA is shown in red. Bar, 100 μm. (I) Graph showing the total area of GFP-expressing cells in eye imaginal discs in which the indicated transgenes and GFP were driven by *dpp-GAL4* relative to the total area of GFP$^+$ tissue in eye-antennal imaginal discs of *dpp-GAL4/UAS-GFP* flies. *ras*^{DN}: *ras* dominant negative; *raf*^{DN}: *raf* dominant negative. ****P-value $< 1 \times 10^{-10}$; N.S., not significant. Quantification assays were performed on eye-antennal discs taken from female larvae. $N \geq 7$ for each genotype in I. Error bars indicate 95% confidence intervals.

versions of *ras* or *raf* failed to elicit overgrowth of GFP$^+$ tissue (Figure 6I; Figure S4). Similarly, coexpression of *ras*^{V12} with RNAi constructs for two RNA metabolism genes—the RNA export factor *short bristles* (*sbr*) or the *Drosophila* ortholog of the Rop-1 RNA binding protein (CG10803)—had no effect on the size of GFP$^+$ tissue above that seen for *ras*^{V12} alone (Figure 6, G–I; Figure S4). Thus, we observed enhanced tissue growth in multiple developmental contexts specifically in genetic combinations marked by reduced *dis3* activity and elevated *ras* or *raf* activity.

We next used the Fly-FUCCI system (Zielke *et al.* 2014) to measure the proportion of cells in G1, S, or G2/M in wild-type wings and in wings with reduced *dis3* activity, elevated *Ras* activity, or both (Figure 7; Table S1). As shown previously (Prober and Edgar 2000), elevating *Ras* activity accelerates cells through G1/S and they stack up in G2/M, resulting in a decreased fraction of cells in G1 and an increased fraction of cells in G2/M relative to wild type. Depletion of *dis3* activity alone also led to a clear increased fraction of cells in G2/M. But, simultaneously reducing *dis3* activity and elevating *Ras* activity dramatically decreased the fraction of cells in G2/M and increased the fraction of cells in S phase relative to either single mutant or wild type (Table S1). We infer that simultaneously reducing *dis3* activity and elevating *Ras* activity drives cells more quickly through G2/M even though either genetic insult on its own causes cells to accumulate in G2/M.

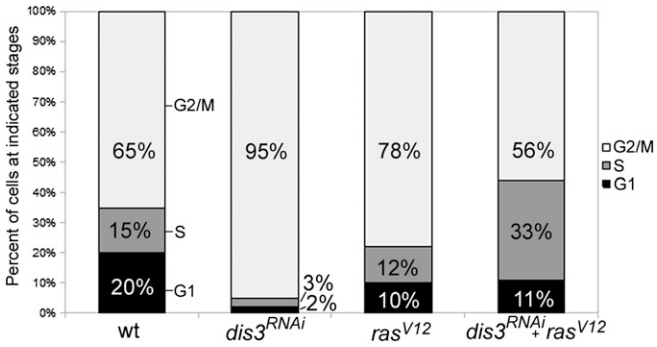

Figure 7 *dis3* and *ras* cooperate to accelerate cells through the G2/M phase. Graph shows the relative percentage of cells of the indicated genotype in the G1, S, and G2/M phases of the cell cycle. All analysis was conducted on wing imaginal discs obtained from late wandering third instar larvae heterozygous for *MS1096-GAL4*, *UAS-CFP::E2F*, *UAS-VenusNLS::CycB*, and the indicated UAS-linked $dis3^{RNAi}$ and/or ras^{V12} transgenes.

dis3 genetic interacts with ras in worms

To test if the genetic interaction between *dis3* and *ras* is conserved, we turned to the *C. elegans* and mouse systems. In *C. elegans*, the Ras–ERK pathway regulates oocyte number and size: reduced *let-60/ras* activity results in fewer, larger oocytes; increased activity results in more, smaller oocytes (Lee *et al.* 2007). To determine if *dis3* genetically interacts with the Ras–ERK pathway during *C. elegans* oogenesis, we took advantage of the $let\text{-}60^{ga89}$ temperature-sensitive gain-of-function allele. At permissive temperature with and without control RNAi-treatment, the germ lines of worms that carry $let\text{-}60^{ga89}$ exhibit elevated levels of dpERK in the germline, but yield a morphologically wild-type linear row of five oocytes at 24 hr past the last larval stage (Figure 8A) (Lee *et al.* 2007). Germ line-specific depletion of *dis3* activity in wild-type worms also resulted in a morphologically wild-type linear row of five oocytes at this stage (Figure 8A). In contrast, when we carried out germ-line-specific depletion of *dis3* activity at the permissive temperature in worms that carried the $let\text{-}60^{ga89}$ allele, we observed a disorganized cluster of 14–20 oocytes in the germ line (Figure 8A, arrowheads). This phenotype is normally only observed in $let\text{-}60^{ga89}$ worms raised at restrictive temperature, suggesting that reduction of *dis3* activity and elevation of *let-60/ras* activity genetically interact in worms to regulate oocyte number and size, as they do in flies to regulate cell division.

Reduction of dis3 function enhances murine B cell proliferation under growth stimulatory conditions

In humans, mutations in *dis3* are found recurrently in multiple myeloma, a tumor of plasma B cells. *In vitro* studies of the most common *dis3* mutations in multiple myeloma appear to reduce but not eliminate *dis3* function (Tomecki *et al.* 2014). Thus, we sought to test whether reducing *dis3* function increased proliferation in a relevant B cell context in the presence of proliferative signals and increased ERK activation. We validated a panel of shRNAs targeting murine *Dis3* for robust knockdown of messenger RNA (mRNA) and protein (Figure 8B) and then tested the effect of dis3 knockdown on naive B cell proliferation following LPS and IL-4 stimulation, which trigger the normally quiescent B cells to divide and undergo class switch recombination. For constitutive Ras signaling, naive B cells were isolated from C57BL/KaLwRij *AID-Cre; LSL-*$Kras^{+/+}$ and *AID-Cre;LSL-*$Kras^{G12D/+}$ mice. These mice harbor the oncogenic $Kras^{G12D}$ allele silenced by a "*lox-stop-lox*" cassette, which is removed by Cre-mediated recombination in B cells undergoing class switch recombination. When we infected $Kras^{+/+}$ B cells with lentiviruses expressing *dis3* shRNAs and monitored cell proliferation, we observed a significant increase in B cell growth relative to empty-vector transduced cells (Figure 8B). When we depleted *dis3* function in $Kras^{G12D/+}$-expressing B cells, we also observed an increase in B cell growth relative to either $Kras^{G12D/+}$-expressing cells or *dis3*-depleted cells alone, but this increase did not reach statistical significance (Figure 8B). We infer that under specific growth stimulatory conditions reduction of *dis3* can enhance cell proliferation from flies to mice.

Discussion

Dis3's apparent role in multiple myeloma has been confounding. It is one of the most frequently mutated genes in multiple myeloma, and these mutations appear to reduce Dis3 activity (Chapman *et al.* 2011; Walker *et al.* 2012; Lohr *et al.* 2014). But, reduction of *dis3* function in yeast leads to a failure or delay in mitosis (Ohkura *et al.* 1988; Kinoshita *et al.* 1991), and studies in vertebrate cell lines using the multiple myeloma-specific Dis3 mutations indicate they reduce, rather than enhance, cell growth and proliferation (Tomecki *et al.* 2014). Our work in flies extends these findings: elimination or strong reduction of *dis3* function or specifically of its exonuclease activity inhibits mitotic cell division. On the other hand, mild reduction of *dis3* function enhances cell proliferation in the presence of elevated Ras–ERK signaling activity in some tissues. Through pilot studies in worms and mice, we confirmed that *dis3* and *ras* interact in worms and that reduction of *dis3* function can enhance cell proliferation in murine plasma B cells, a cell type directly relevant to multiple myeloma, at least under growth stimulatory conditions. Thus, our work provides clear experimental evidence that reduction, not elimination, of *dis3* function can, in specific contexts, enhance cell proliferation.

Clearly, *dis3* function must exceed some threshold for cells to divide, a characteristic of many genes. But, how might reduction of *dis3* function enhance cell proliferation? Here, we draw a parallel to *dis2/PP1*, a gene that displays similar cell cycle phenotypes to *dis3* in *S. pombe* and flies (Ohkura *et al.* 1988; Axton *et al.* 1990). During mitosis, Dis2/PP1 activity is thought to prevent chromosome separation until all chromosome pairs are bioriented on the mitotic spindle (Vanoosthuyse and Hardwick 2009; Meadows *et al.*, 2011); once this criterion is met, its activity is thought to be directly

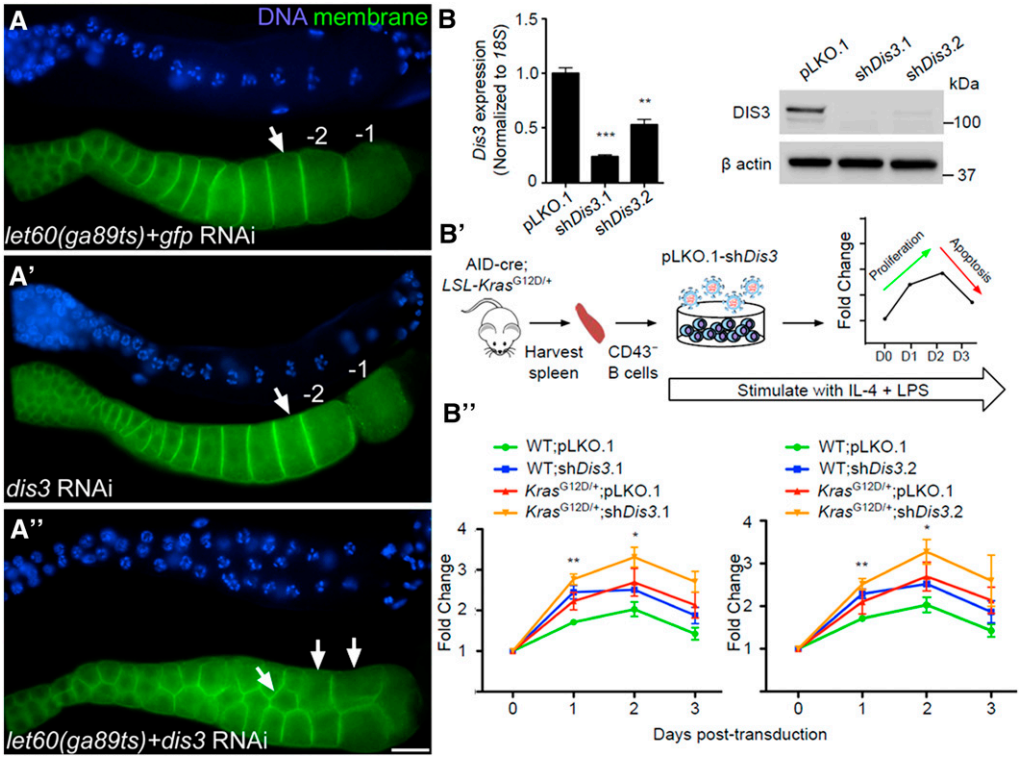

Figure 8 Reduction of *dis3* function enhances cell proliferation in mice. (A) *dis3* and *ras* interact in the *C. elegans* germ line. Proximal region of *C. elegans* germ lines of indicated genotypes labeled for DNA (blue) and cell membranes (green). (A) Attenuated germ-line-specific RNAi of *dis3* in an *rrf-1*^{pk1417} background yields oocytes (arrow) of wild-type size and morphology; the *rrf-1* mutant prevents RNAi in the soma but not the germ line (Sijen *et al.* 2001). (A′) At permissive temperature, germ lines of *let-60/ras*^{ga89ts} worms also exhibit wild-type oocyte size and morphology. (A′′) At permissive temperature, reduction of *dis3* function in the *let-60/ras*^{ga89ts} background leads to a small oocyte phenotype. Bar, 20 μm. (B) *dis3* knockdown drives hyper-proliferation of murine splenic naive B cells. (B) Validation of shRNAs targeting murine *Dis3* mRNA by qPCR and immunoblot of DIS3 in *Arf*$^{-/-}$ mouse embryonic fibroblasts transduced with empty pLKO.1 or one of two sh*Dis3* constructs. *18S* was used for qPCR normalization, and β-actin as a loading control for immunoblots. (B′) Outline of experimental approach. CD43^{-} splenic naive B cells were isolated from KaLwRij *AID-Cre*; *LSL-Kras*$^{G12D/+}$ or *AID-Cre*; *LSL-Kras*$^{+/+}$ spleens and stimulated with IL-4 and LPS for 24 hr. Cells were then transduced and cell numbers counted on successive days. (B′′) Growth curves of *AID-Cre*; *LSL-Kras*$^{+/+}$ and *AID-Cre*; *LSL-Kras*$^{G12D/+}$ CD43^{-} splenic B cells transduced with empty pLKO.1 or one of two sh*Dis3* constructs (n = 3). Asterisks in B′′ correspond to *Dis3* knockdown in *Kras*$^{+/+}$ cells *vs.* empty vector control in the same background. Error bars indicate SEM. *$P < 0.05$, **$P < 0.005$, ***$P < 0.0005$, using Student's *t*-test.

inhibited by CDK1-mediated phosphorylation (Yamano *et al.* 1994; Kwon *et al.* 1997; Trinkle-Mulcahy *et al.* 2003), and chromosome separation and anaphase commence. Thus, Dis2 activity must be on and then off at sequential stages of the cell cycle for the cell to cycle normally. Pharmacological inhibition of PP1 in cycling *Xenopus* embryo extracts has been shown to trigger premature mitotic entry (Walker *et al.* 1992). We speculate that, like Dis2, the activity of Dis3 is regulated during the cell cycle, with our work raising, but not definitely answering, the contention that CDK1 turns Dis3 activity off during mitosis. Our FUCCI data support a role for *dis3* in delaying progress through G2/M at least in the presence of elevated Ras activity, which by itself accelerates cells through G1–S, causing them to stack up in G2/M. As observed for Dis2/PP1, diminution of *dis3* activity might then trigger premature mitotic entry at least under specific growth stimulatory conditions. In support of this idea, Dis3 associates with Ran and RCC1 (Noguchi *et al.* 1996), and mutations in each gene have been shown to trigger premature mitotic entry in yeast (Matsumoto and Beach 1991). As RCC1 associates with chromatin, recent work by Eberle *et al.* (2015) and prior work in yeast that identify a function for *dis3* in heterochromatic gene silencing (Murakami *et al.* 2007) hint that *dis3* could regulate cell cycle progression via an epigenetic mechanism. Significant work is needed to clarify how Dis3 regulates cell cycle progression, but we note that the combination of elevated Ras activity and reduced *dis3* activity may allow cells to accelerate through both G1–S and G2–M transitions, providing a recipe, or at least predisposition, for deregulated cell and tissue growth.

Dis3's exonuclease, not endonuclease, activity appears critical for its cell cycle function. In flies, Dis3's exonuclease activity is required for mitotic cells to grow and divide (but not for endoreduplicative cells to grow). In humans, most multiple myeloma-specific mutations in *dis3* cluster in its exonuclease domain and appear to reduce, but not eliminate, Dis3 exonuclease activity (Chapman *et al.* 2011; Walker *et al.* 2012; Lohr *et al.* 2014; Tomecki *et al.* 2014). Thus, Dis3 likely mediates its effects on cell division via exonucleolytic degradation or modification of specific RNA species that regulate cell cycle progression. Clearly, Dis3 could control the cell cycle by targeting individual mRNAs or micro RNAs (miRNAs). In support of this idea, in human myeloma cell lines and mouse NIH3T3 cells, reduction of *dis3* activity appears to decrease *let-7* miRNA expression, causing increased expression of *let-7* target genes, including *ras* and *myc* (Segalla *et al.* 2015). In fly wing imaginal discs, knockdown of *dis3* mRNA modestly decreases *let-7* miRNA expression (Towler *et al.* 2015), but in our hands reducing *let-7* activity by itself in the fly ovary, via expression of a *let-7* miRNA

sponge, did not recapitulate the posterior follicle cell overproliferation phenotype observed in *dis3* hypomorphic backgrounds (M. J. Snee and J. B. Skeath, unpublished observations). An alternative, nonmutually exclusive model is that *dis3* might regulate cell division epigenetically. In yeast, Dis3 has been shown to associate with centromeric-repeat DNA, promote heterochromatin silencing at centromeres, and inhibit accumulation of noncoding centromeric repeat RNAs (Murakami *et al.* 2007; Bernard *et al.* 2010). Moreover, small centromeric RNAs have been shown to regulate centromere formation and function in human cells and maize (Topp *et al.* 2004; Wong *et al.* 2007). Additional experimental data are needed to support either model with future work focusing on the identification of RNAs bound by Dis3 and the elucidation of the function of these RNAs or their encoded products on cell cycle progression.

Acknowledgments

We thank Doug Chalker, Sally Elgin, Tim Schedl, and Susan Dutcher for helpful discussions and/or critical review of the manuscript and Trudi Schüpbach, Lori Wallrath, Sally Elgin, Paul Macdonald, Greg Longmore, Kathy Matthews, Kevin Cook, the Iowa Developmental Studies Hybridoma Bank (Eunice Kennedy Shriver National Institute of Child Health and Human Development), and the Bloomington Stock Center for reagents and/or fly strains. This research was funded by grants from the National Institutes of Health (NIH) (GM98200) and the American Cancer Society (RSG-14-044-01-DDC) to S.A., an NIH grant (R01CA175349) to M.H.T., and a National Science Foundation grant (IOS-0744261) and an NIH grant (NS036570) to J.B.S. The funders had no role in study design, data collection and analysis, decision to publish, or preparation of the manuscript.

Literature Cited

Aoki, K., Y. Nakaseko, K. Kinoshita, G. Goshima, and M. Yanagida, 2006 CDC2 phosphorylation of the fission yeast dis1 ensures accurate chromosome segregation. Curr. Biol. 16: 1627–1635.

Arraiano, C. M., R. G. Matos, and A. Barbas, 2010 RNase II: the finer details of the Modus operandi of a molecular killer. RNA Biol. 7: 276–281.

Arur, S., and T. Schedl, 2014 Generation and purification of highly specific antibodies for detecting post-translationally modified proteins in vivo. Nat. Protoc. 9: 375–395.

Arur, S., M. Ohmachi, S. Nayak, M. Hayes, A. Miranda *et al.*, 2009 Multiple ERK substrates execute single biological processes in *Caenorhabditis elegans* germ-line development. Proc. Natl. Acad. Sci. USA 106: 4776–4781.

Axton, J. M., V. Dombradi, P. T. Cohen, and D. M. Glover, 1990 One of the protein phosphatase 1 isoenzymes in Drosophila is essential for mitosis. Cell 63: 33–46.

Becalska, A. N., and E. R. Gavis, 2010 Bazooka regulates microtubule organization and spatial restriction of germ plasm assembly in the *Drosophila* oocyte. Dev. Biol. 340: 528–538.

Bernard, P., J. Drogat, S. Dheur, S. Genier, and J. P. Javerzat, 2010 Splicing factor Spf30 assists exosome-mediated gene silencing in fission yeast. Mol. Cell. Biol. 30: 1145–1157.

Brand, A. H., and N. Perrimon, 1993 Targeted gene expression as a means of altering cell fates and generating dominant phenotypes. Development 118: 401–415.

Buhler, M., W. Haas, S. P. Gygi, and D. Moazed, 2007 RNAi-dependent and -independent RNA turnover mechanisms contribute to heterochromatic gene silencing. Cell 129: 707–721.

Chan, F. L., O. J. Marshall, R. Saffery, B. W. Kim, E. Earle *et al.*, 2012 Active transcription and essential role of RNA polymerase II at the centromere during mitosis. Proc. Natl. Acad. Sci. USA 109: 1979–1984.

Chapman, M. A., M. S. Lawrence, J. J. Keats, K. Cibulskis, C. Sougnez *et al.*, 2011 Initial genome sequencing and analysis of multiple myeloma. Nature 471: 467–472.

Cullen, C. F., P. Deak, D. M. Glover, and H. Ohkura, 1999 *mini spindles:* a gene encoding a conserved microtubule-associated protein required for the integrity of the mitotic spindle in *Drosophila*. J. Cell Biol. 146: 1005–1018.

Dziembowski, A., E. Lorentzen, E. Conti, and B. Seraphin, 2007 A single subunit, Dis3, is essentially responsible for yeast exosome core activity. Nat. Struct. Mol. Biol. 14: 15–22.

Eberle, A. B., A. Jordán-Pla, A. Gañez-Zapater, V. Hessle, G. Silberberg *et al.*, 2015 An interaction between RRP6 and SU(VAR)3–9 targets RRP6 to heterochromatin and contributes to heterochromatin maintenance in *Drosophila melanogaster*. PLoS Genet. 11: e1005523.

Fanti, L., and S. Pimpinelli, 2004 Analysis of mitosis in squash preparations of larval brains: orcein, Giemsa, Hoechst 33258, DAPI, quinacrine, and N-banding. Methods Mol. Biol. 247: 325–332.

Fernandez, A., D. L. Brautigan, and N. J. Lamb, 1992 Protein phosphatase type 1 in mammalian cell mitosis: chromosomal localization and involvement in mitotic exit. J. Cell Biol. 116: 1421–1430.

Folco, H. D., A. L. Pidoux, T. Urano, and R. C. Allshire, 2008 Heterochromatin and RNAi are required to establish CENP-A chromatin at centromeres. Science 319: 94–97.

Gabay, L., R. Seger, and B. Z. Shilo, 1997 MAP kinase in situ activation atlas during Drosophila embryogenesis. Development 124: 3535–3541.

Gatti, M., and B. S. Baker, 1989 Genes controlling essential cell-cycle functions in Drosophila melanogaster. Genes Dev. 3: 438–453.

Gergely, F., V. M. Draviam, and J. W. Raff, 2003 The ch-TOG/XMAP215 protein is essential for spindle pole organization in human somatic cells. Genes Dev. 17: 336–341.

Goode, S., and N. Perrimon, 1997 Inhibition of patterned cell shape change and cell invasion by Discs large during *Drosophila* oogenesis. Genes Dev. 11: 2532–2544.

Hou, D., M. Ruiz, and E. D. Andrulis, 2012 The ribonuclease Dis3 is an essential regulator of the developmental transcriptome. BMC Genomics 13: 359.

Kinoshita, N., M. Goebl, and M. Yanagida, 1991 The fission yeast dis3+ gene encodes a 110-kDa essential protein implicated in mitotic control. Mol. Cell. Biol. 11: 5839–5847.

Kiss, D. L., and E. D. Andrulis, 2010 Genome-wide analysis reveals distinct substrate specificities of Rrp6, Dis3, and core exosome subunits. RNA 16: 781–791.

Kwon, Y. G., S. Y. Lee, Y. Choi, P. Greengard, and A. C. Nairn, 1997 Cell cycle-dependent phosphorylation of mammalian protein phosphatase 1 by cdc2 kinase. Proc. Natl. Acad. Sci. USA 94: 2168–2173.

Lebreton, A., R. Tomecki, A. Dziembowski, and B. Seraphin, 2008 Endonucleolytic RNA cleavage by a eukaryotic exosome. Nature 456: 993–996.

Lee, M. H., M. Ohmachi, S. Arur, S. Nayak, R. Francis *et al.*, 2007 Multiple functions and dynamic activation of MPK-1 extracellular signal-regulated kinase signaling in *Caenorhabditis elegans* germline development. Genetics 177: 2039–2062.

Lohr, J. G., P. Stojanov, S. L. Carter, P. Cruz-Gordillo, M. S. Lawrence *et al.*, 2014 Widespread genetic heterogeneity in multiple myeloma: implications for targeted therapy. Cancer Cell 25: 91–101.

Mamolen, M., A. Smith, and E. D. Andrulis, 2011 *Drosophila melanogaster* Dis3 N-terminal domains are required for ribonuclease activities, nuclear localization and exosome interactions. Nucleic Acids Res. 38: 5507–5517.

Matsumoto, T., and D. Beach, 1991 Premature initiation of mitosis in yeast lacking RCC1 or an interacting GTPase. Cell 66: 347–360.

Meadows, J. C., L. A. Shepperd, V. Vanoosthuyse, T. C. Lancaster, A. M. Sochaj *et al.*, 2011 Spindle checkpoint silencing requires association of PP1 to both Spc7 and kinesin-8 motors. Dev. Cell 20: 739–750.

Mitchell, P., E. Petfalski, A. Shevchenko, M. Mann, and D. Tollervey, 1997 The exosome: a conserved eukaryotic RNA processing complex containing multiple 3′→5′ exoribonucleases. Cell 91: 457–466.

Murakami, H., D. B. Goto, T. Toda, E. S. Chen, S. I. Grewal *et al.*, 2007 Ribonuclease activity of Dis3 is required for mitotic progression and provides a possible link between heterochromatin and kinetochore function. PLoS One 2: e317.

Murphy, L. O., and J. Blenis, 2006 MAPK signal specificity: the right place at the right time. Trends Biochem. Sci. 31: 268–275.

Nabeshima, K., H. Kurooka, M. Takeuchi, K. Kinoshita, Y. Nakaseko *et al.*, 1995 p93dis1, which is required for sister chromatid separation, is a novel microtubule and spindle pole body-associating protein phosphorylated at the Cdc2 target sites. Genes Dev. 9: 1572–1585.

Neuman-Silberberg, F. S., and T. Schüpbach, 1993 The Drosophila dorsoventral patterning gene *gurken* produces a dorsally localized RNA and encodes a TGF alpha-like protein. Cell 75: 165–174.

Nigg, E. A., 2001 Mitotic kinases as regulators of cell division and its checkpoints. Nat. Rev. Mol. Cell Biol. 2: 21–32.

Nilson, L. A., and T. Schüpbach, 1999 EGF receptor signaling in *Drosophila* oogenesis. Curr. Top. Dev. Biol. 44: 203–243.

Noguchi, E., N. Hayashi, Y. Azuma, T. Seki, M. Nakamura *et al.*, 1996 Dis3, implicated in mitotic control, binds directly to Ran and enhances the GEF activity of RCC1. EMBO J. 15: 5595–5605.

Ohkura, H., Y. Adachi, N. Kinoshita, O. Niwa, T. Toda *et al.*, 1988 Cold-sensitive and caffeine-supersensitive mutants of the Schizosaccharomyces pombe dis genes implicated in sister chromatid separation during mitosis. EMBO J. 7: 1465–1473.

Ohkura, H., N. Kinoshita, S. Miyatani, T. Toda, and M. Yanagida, 1989 The fission yeast dis2+ gene required for chromosome disjoining encodes one of two putative type 1 protein phosphatases. Cell 57: 997–1007.

Prober, D. A., and B. A. Edgar, 2000 Ras1 promotes cellular growth in the Drosophila wing. Cell 100: 435–446.

Rorth, P., 1996 A modular misexpression screen in Drosophila detecting tissue-specific phenotypes. Proc. Natl. Acad. Sci. USA 93: 12418–12422.

Rosic, S., F. Kohler, and S. Erhardt, 2014 Repetitive centromeric satellite RNA is essential for kinetochore formation and cell division. J. Cell Biol. 207: 673.

Schaeffer, D., B. Tsanova, A. Barbas, F. P. Reis, E. G. Dastidar *et al.*, 2009 The exosome contains domains with specific endoribonuclease, exoribonuclease and cytoplasmic mRNA decay activities. Nat. Struct. Mol. Biol. 16: 56–62.

Segalla, S., S. Pivetti, K. Todoerti, M. A. Chudzik, E. C. Giuliani *et al.*, 2015 The ribonuclease DIS3 promotes let-7 miRNA maturation by degrading the pluripotency factor LIN28B mRNA. Nucleic Acids Res. 43: 5182–5193.

Sijen, T., J. Fleenor, F. Simmer, K. L. Thijssen, S. Parrish *et al.*, 2001 On the role of RNA amplification in dsRNA-triggered gene silencing. Cell 107: 465–476.

Tomecki, R., K. Drazkowska, and A. Dziembowski, 2010 Mechanisms of RNA degradation by the eukaryotic exosome. ChemBioChem 11: 938–945.

Tomecki, R., K. Drazkowska, I. Kucinski, K. Stodus, R. J. Szczesny *et al.*, 2014 Multiple myeloma-associated hDIS3 mutations cause perturbations in cellular RNA metabolism and suggest hDIS3 PIN domain as a potential drug target. Nucleic Acids Res. 42: 1270–1290.

Topp, C. N., C. X. Zhong, and R. K. Dawe, 2004 Centromere-encoded RNAs are integral components of the maize kinetochore. Proc. Natl. Acad. Sci. USA 101: 15986–15991.

Towler, B. P., C. I. Jones, S. C. Viegas, P. Apura, J. A. Waldron *et al.*, 2015 The 3′-5′ exoribonuclease Dis3 regulates the expression of specific microRNAs in *Drosophila* wing imaginal discs. RNA Biol. 12: 728–741.

Trinkle-Mulcahy, L., P. D. Andrews, S. Wickramasinghe, J. Sleeman, A. Prescott *et al.*, 2003 Time-lapse imaging reveals dynamic relocalization of PP1γ throughout the mammalian cell cycle. Mol. Biol. Cell 14: 107–117.

Vanoosthuyse, V., and K. G. Hardwick, 2009 A novel protein phosphatase 1-dependent spindle checkpoint silencing mechanism. Curr. Biol. 19: 1176–1181.

Verdel, A., S. Jia, S. Gerber, T. Sugiyama, S. Gygi *et al.*, 2004 RNAi-mediated targeting of heterochromatin by the RITS complex. Science 303: 672–676.

Volpe, T. A., C. Kidner, I. M. Hall, G. Teng, S. I. Grewal *et al.*, 2002 Regulation of heterochromatic silencing and histone H3 lysine-9 methylation by RNAi. Science 297: 1833–1837.

Walker, B. A., C. P. Wardell, L. Melchor, S. Hulkki, N. E. Potter *et al.*, 2012 Intraclonal heterogeneity and distinct molecular mechanisms characterize the development of t(4;14) and t(11;14) myeloma. Blood 120: 1077–1086.

Walker, D. H., A. A. DePaoli-Roach, and J. L. Maller, 1992 Multiple roles for protein phosphatase 1 in regulating the Xenopus early embryonic cell cycle. Mol. Biol. Cell 3: 687–698.

Wong, L. H., K. H. Brettingham-Moore, L. Chan, J. M. Quach, M. A. Anderson *et al.*, 2007 Centromere RNA is a key component for the assembly of nucleoproteins at the nucleolus and centromere. Genome Res. 17: 1146–1160.

Yamano, H., K. Ishii, and M. Yanagida, 1994 Phosphorylation of dis2 protein phosphatase at the C-terminal cdc2 consensus and its potential role in cell cycle regulation. EMBO J. 13: 5310–5318.

Zielke, N., J. Korzelius, M. van Straaten, K. Bender, G. F. Schuhknecht *et al.*, 2014 Fly-FUCCI: a versatile tool for studying cell proliferation in complex tissues. Cell Reports 7: 588–598.

Communicating editor: D. I. Greenstein

GENETICS

Supporting Information
www.genetics.org/lookup/suppl/doi:10.1534/genetics.116.187930/-/DC1

Collaborative Control of Cell Cycle Progression by the RNA Exonuclease Dis3 and Ras Is Conserved Across Species

Mark J. Snee, William C. Wilson, Yi Zhu, Shin-Yu Chen, Beth A. Wilson, Cedric Kseib, Julie O'Neal, Nitin Mahajan, Michael H. Tomasson, Swathi Arur, and James B. Skeath

DOI: 10.1534/genetics.116.187930

Figure S1:

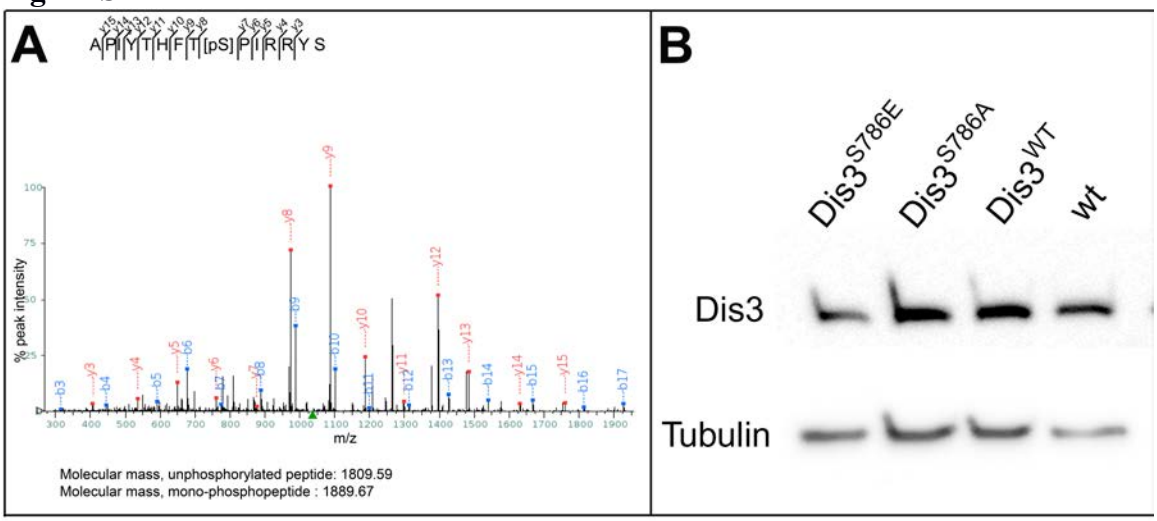

Fig. S1. Comparable expression of the wild-type, phospho-mimetic, and non-phosphorylatable forms of Dis3 in late third instar larvae.

A) Sequest Mass Spectral chart of the phosophorylated DIS3 peptide. The DIS3 peptide APIYTHFT[pS]PIRRY was identified by phospho-proteomics approach as a mono-phosphorylated peptide. X-axis represents the molecular mass and charge ratio of each amino-acid in the phospho-peptide; Y-axis represents percent peak intensity of each amino-acid. The "y" ions are calculated from C terminal to N-terminal of the peptide. The phosphate group increased the molecular mass by 80 units, when compared to the unphosphorylated peptide. B) Lanes 1-3: Western blot of Dis3 protein levels in protein extracts obtained from *dis3*^{1}/*dis3*^{2} late third instar larvae in which the indicated UAS-linked *dis3* transgene (Dis3^{S786E}, Dis3^{S786A}, or Dis3^{WT}) was driven under the control of Tubulin-GAL4; Lane 4: Dis3 protein levels in extracts obtained from wild-type late-third instar larvae. Beta-tubulin protein levels are shown for loading controls. The levels of Dis3 protein as driven by each of the three *dis3* transgenes appears comparable; note that the three dis3 transgenes are inserted into the identical chromosomal location.

Figure S2:

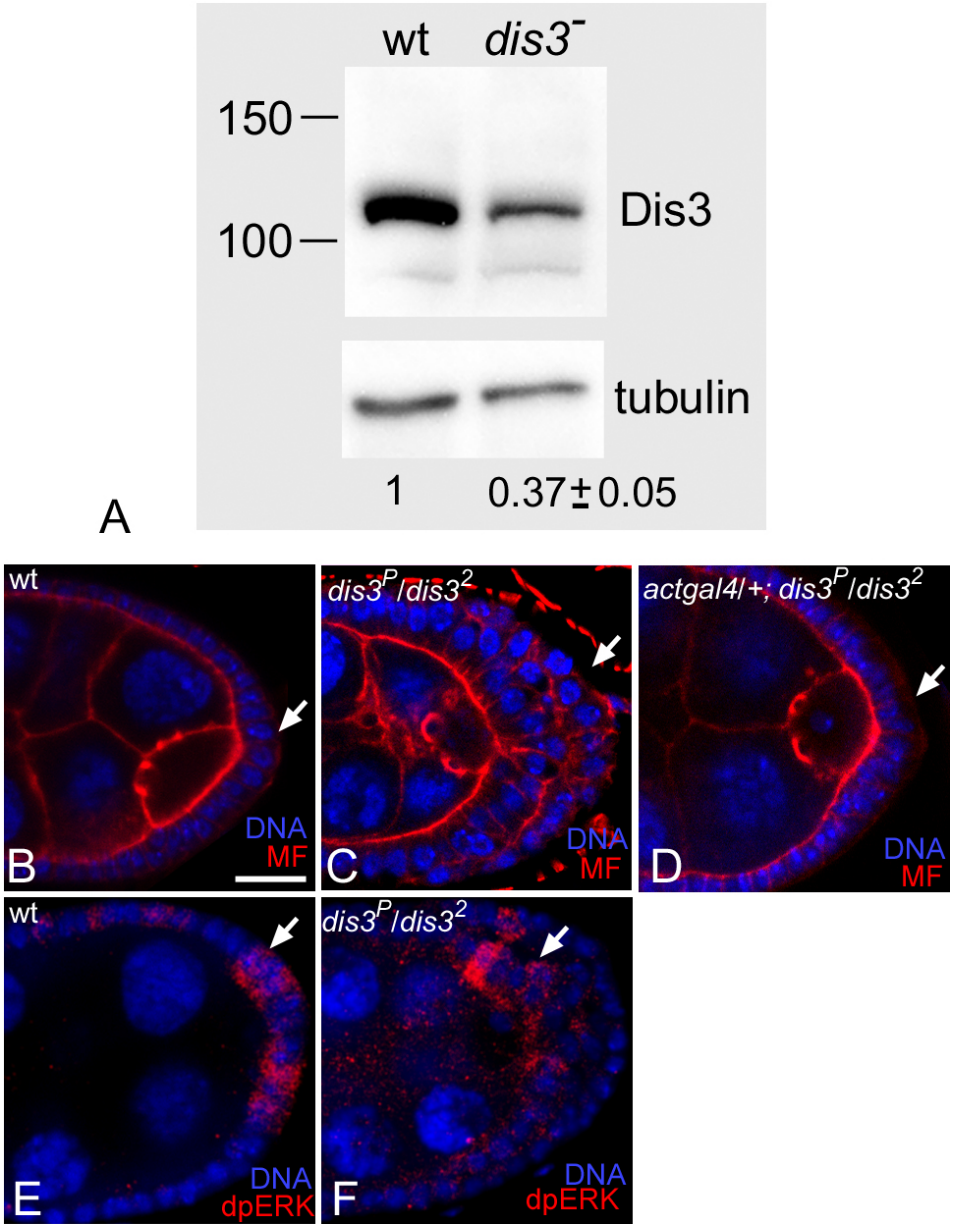

Fig S2. Reduction of *dis3* function induces posterior follicle cell overproliferation, but not excess dpERK activation. (A) Western blot of Dis3 protein in protein extracts obtained from wild-type or $dis3^{G5039}$/ $dis3^{2}$ ($dis3^{-}$) mutant ovaries. Dis3 protein is expressed at 38±5% of wild-type levels in $dis3^{-}$ mutant ovaries; quantification was performed on three independent western blot assays, using beta-tubulin levels for normalization of protein levels. (B-F) High magnification views of the posterior portion of *Drosophila* egg chambers from wild-type (B, E), $dis3^{P}/dis3^{2}$ mutant (C, F), and *actin-gal4*/+; $dis3^{P}/dis3^{2}$ mutant (D) females stained for DNA (blue B-F), microfilaments (red; B-D), and dpERK (red; E, F). Arrows in B-F point to posterior follicle cells.

Figure S3:

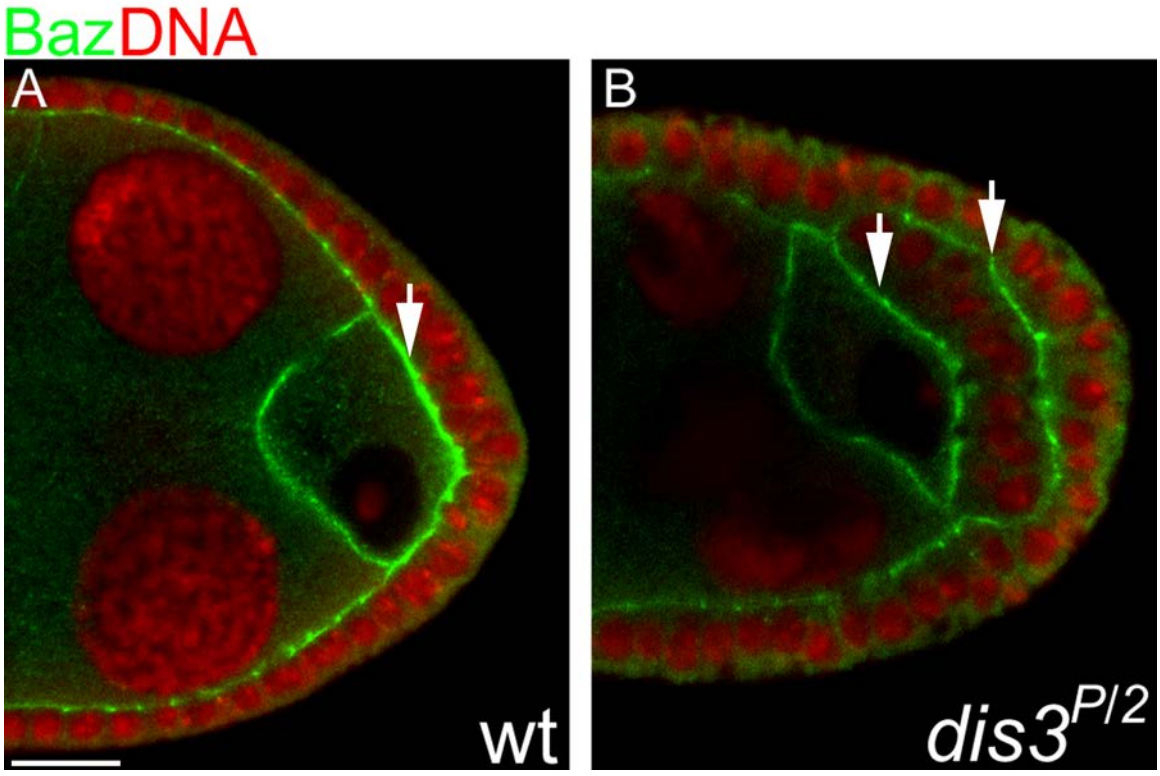

Fig. S3. Reduction of *dis3* function does not alter follicle cell polarity. (A,B) High magnification views of the posterior portion of *Drosophila* egg chambers from wild-type (A) and $dis3^{P}/dis3^{2}$ mutant (B) females stained for DNA (red) and Bazooka (green). Arrows point to posterior follicle cells with apically localized Bazooka. Scale bar is 10 μm.

Figure S4:

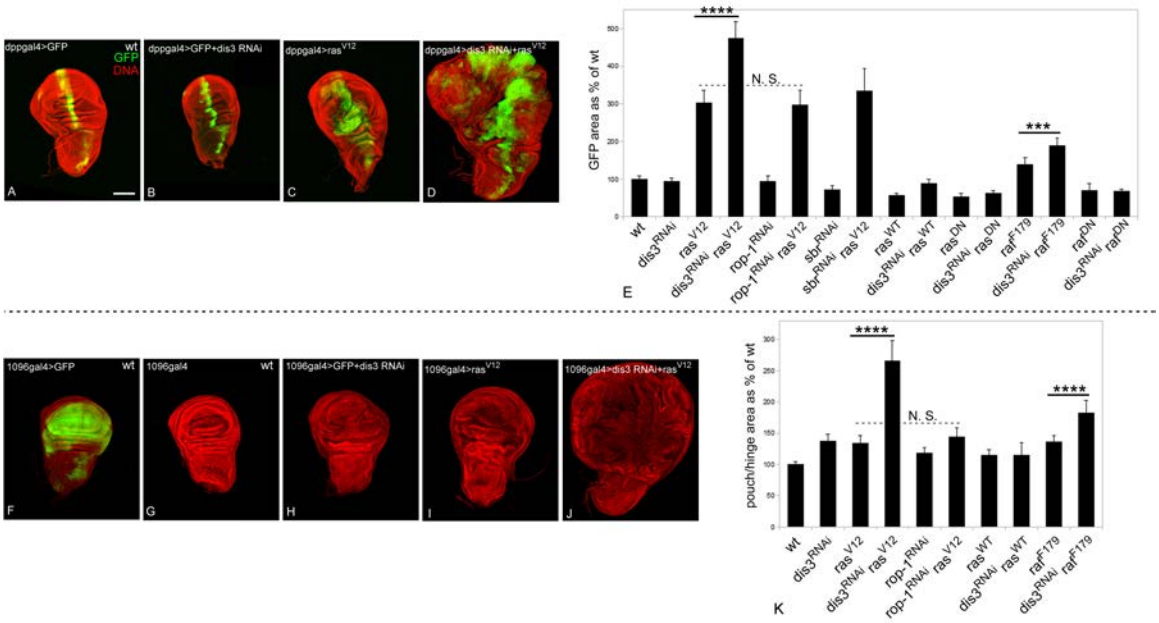

Fig. S4. *dis3* collaborates with *ras* and *raf* to drive tissue overgrowth. (A-D) Wing imaginal discs in which the indicated UAS-linked transgenes were driven under the control of the *dpp-GAL4* driver: (A) *UAS-GFP*, (B) *UAS-GFP, UAS-dis3*^{RNAi}, (C) *UAS-GFP, UAS-ras*^{V12}, and (D) *UAS-GFP, UAS-dis3*^{RNAi}, *UAS-ras*^{V12}. The region in which the transgenes are expressed is indicated by GFP expression (green); DNA is labeled in red. (E) Graph showing the quantification of the total GFP^{+} area in wing imaginal discs in which the indicated transgenes are driven under the control of *dpp-GAL4* relative to the total GFP^{+} area observed in wild-type wing discs (*dppGAL4>GFP*). (F-J) Wing imaginal discs in which the indicated UAS-linked transgenes were driven under the control of the *1096-GAL4* driver line: (F) *UAS-GFP*, (G) none, (H) *UAS-GFP, UAS-dis3*^{RNAi}, (I) *UAS-ras*^{V12}, and (D) *UAS-dis3*^{RNAi}, *UAS-ras*^{V12}. In F, GFP expression (green) highlights the region, the pouch/hinge region, in which *1096-GAL4* drives transgene expression; DNA is labeled in red. (K) Graph showing the quantification of the total GFP^{+} area in wing imaginal discs in which the indicated transgenes are driven by *1096-GAL4* relative to the total GFP^{+} area observed in wild-type wing discs (*1096-GAL4>GFP*). Co-expression of the *dis3*^{RNAi} transgene with constitutively active, but not wild-type or dominant-negative, forms of ras or raf lead to tissue over-growth phenotypes; over-growth phenotypes are not observed upon co-expression of RNAi transgenes for other RNA metabolism genes (*rop-1*, *sbr*) with *ras* or *raf* (E, K). Error bars show 95% confidence interval. N.S. indicates a non significant difference; "***" indicates a P value less than 0.001, and "****" indicates a P value less than 0.0001 (Student's T test). N is $\geq$ 9 for each genotype; scale bar is 100 μm.

Table S1. *dis3* and *ras* interact to promote G2/M transition

GENOTYPE [a]	G1	S	G2/M
wild type	19.6 ± 5.3%	15.0 ± 7.1%	65.4 ± 4.5%
dis3 RNAi	1.8 ± 1.5%	3.5 ± 1.6%	94.6 ± 2.1% **
ras^{V12}	10.0 ± 6.3%	11.6 ± 5.9%	78.4 ± 9.0% **
dis3 RNAi + ras^{V12}	10.9 ± 7.8%	33.4 ± 10.5%	55.6 ± 8.7% *

Average percentage of cells in G1, S, and G2/M phase (± SD) in the pouch region of wing imaginal discs expressing FUCCI reporters and indicated UAS-transgenes of *dis3* or *ras*. N ≥13 wing discs and 1000 cells scored per genotype.

[a] Female late wandering third instar larvae with *MS1096gal4*/+; *UAS-CFP::E2F*, *UAS-VenusNLS::CycB*/+ and indicated *dis3* and ras^{V12} transgenes.

* Student's t-test $p<1X10^{-3}$ relative to wild type.

** Student's t-test $p<1X10^{-4}$ relative to wild type.